



Progress and perspectives of joints defects of laser-arc hybrid welding: a review

Qingyong Liu¹ · Di Wu^{1,2} · Qingzhao Wang³ · Peilei Zhang^{1,4}  · Hua Yan¹ · Tianzhu Sun⁵ · Ruifeng Li⁶

Received: 1 September 2023 / Accepted: 24 November 2023 / Published online: 6 December 2023
© The Author(s), under exclusive licence to Springer-Verlag London Ltd., part of Springer Nature 2023

Abstract

Laser-arc hybrid welding (LAHW), being a high-efficiency with excellent properties of high welding speed, deep penetration, and good bridging performance, has been paid close attention by domestic and overseas scholars. So far, the lack of suppression and detection of welding defects is still considered the critical technical obstacle that affects its welding quality, particularly for workpieces with industrial requirements. One vital method to conquer this challenging issue is the visual analysis technique with the combination of numerical simulation technique, which has been researched by abundant study outcomes. The primary target of detecting is to collect basic information and to understand the formation mechanism of welding defects. This review firstly describes welding defects online detection technology, such as high-speed image, electrical signal, acoustical signal, and optical signal detection technology. Then much emphasis has been placed on the internal mechanism of forming welding defects, including undercut, humping, porosity, and spatter defects. Particularly, the defect suppression methods are presented in order to restrain and address the welding defect problems. Finally, the current difficulties and potential remedies are discussed to supply an understanding on what still needs to be improved in the LAHW process. This comprehensive review is to offer guidance for those trying to reduce welding defects as they enhance the welding joints' quality.

Keywords Laser-arc hybrid welding · Laser welding · Welding defects · Online detection technology · Suppression methods

1 Introduction

Laser-arc hybrid welding (LAHW) can make full use of the respective characteristics of two heat sources, and obtain welding effects which are superior to single laser welding

and arc welding. Compared with traditional arc welding, LAHW has the superiorities of high welding speed, high efficiency, low welding heat input, and small residual stress of workpieces. At the same time, the addition of a laser heat source can effectively improve the arc stability. Compared with conventional laser welding, LAHW can improve the bridging ability of base metal. In addition, LAHW can also reduce cracks, thermal deformation, and porosity at the welding joints. As an advanced welding technology, the LAHW method has been widely used in a variety of manufacturing [1–5]. However, LAHW is involved in many complicated physical processes, including keyhole effect, molten pool flow, and droplet transfer behavior, which cause quite complex transport phenomena. The welding joint quality will be influenced by these dynamic factors. The potential welding defects will weaken the mechanical properties and fatigue properties of workpieces [6].

The welding states are divided into well welds formation and typical welding defects, including undercuts, humping, porosities, and spatters defects [7–9], as shown in Fig. 1. Due to the coupling effects of multiple fields such as flow field, electromagnetic field, temperature field, and stress field

✉ Di Wu
wudi@sues.edu.cn

✉ Peilei Zhang
peilei@sues.edu.cn

¹ School of Materials Science and Engineering, Shanghai University of Engineering Science, Shanghai 201620, China

² School of Materials Science and Engineering, Shanghai Jiao Tong University, Shanghai 200240, China

³ SANY Heavy Industry Co., Ltd., Shanghai 201306, China

⁴ Jiangsu New Yangzi Shipbuilding Co., Ltd., Jingjiang 214532, China

⁵ Warwick Manufacturing Group (WMG), University of Warwick, Coventry CV4 7AL, UK

⁶ School of Materials Science and Engineering, Jiangsu University of Science and Technology, Zhenjiang 212003, China

in LAHW, as well as the extremely complex heat and mass transfer process of rapid transformation of solid, liquid, and gas states in metal materials, there are many factors affecting welding quality, and process parameters are difficult to control and optimize. The welding process still faces welding defects, such as undercuts, humping, porosities, and spatters, which cause stress concentration or reduction of weld cross-sectional area, weakening the fatigue strength and load-bearing capacity of welded joints, and seriously affecting the reliability and durability of welded structures[10].

LAHW is a common metal-joining method, which is widely used in production and manufacturing. The welding quality determines the strength of the welding joints. When the welds fail, the entire structure usually fails. In order to enhance welding quality, suppress welding defects, and better analyze the generation mechanism of defects, some detecting methods have been proposed to supply accurate and visual information to control joint quality. At present, the design idea of detection technology mainly depends on the coupling interaction of laser and arc heat sources. The interaction between heat sources and workpieces carries all kinds of welding information, such as visual signals, electrical signals, acoustical signals, and optical signals, which have close relations with welding stability and quality. Therefore, the accurate utilization of detection methods is of significance in explaining the internal mechanism of the welding process.

Figure 2 demonstrates the content frame of this review, which consists of two main processes. In fundamental theory (Sections 2, 3, and 4), the synergistic mechanism of laser-arc heat source is deeply researched, and the advantages of LAHW in Section 2 is introduced. Then, to clearly observe the generation of welding defects, different online detection methods are presented, respectively, in Section 3. In addition, it further elaborates on the formation mechanism of main defects in Section 4. In effective measures from Section 5, the suppression methods of welding defects are summarized for analyzing and controlling welding joint quality.

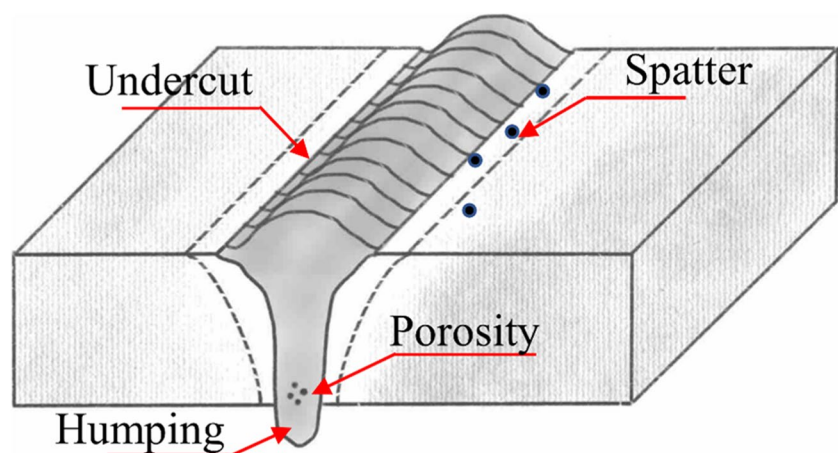
Finally, Section 6 describes the potential difficulties and challenges of LAHW and welding defects, and concludes this review.

2 Laser-arc hybrid welding

The LAHW is a novel welding technology[11], which was first proposed and experimentally studied by Professor Steen in 1978 [12]. The characteristics of different welding methods are summarized in Table 1. As shown in Fig. 3, the LAHW technology integrates the advantages of laser and arc heat sources, which can significantly enhance the quality of weld formation [13–15]. It is one of the most promising fusion welding technologies. Due to the synergistic effect of two heat sources, LAHW technology has many unique advantages over single laser/arc welding, which avoids the problem of insufficient single-heat-source energy. It has the following characteristics:

- (1) It has high efficiency and low energy consumption [16]. In the LAHW process, the surface of the workpieces melts by the arc heat source. Compared to the surface of low-temperature solid base metal, the laser absorption rate is greatly increased, which has a significant improvement effect on the welds' width and depth, reduces the requirement for laser energy, and enhances the welding ability.
- (2) It can improve the microstructure of the weld seam [17–19]. Compared to traditional welding methods, the welding heat input of hybrid welding is lower. It can weld continually with a higher welding speed, the weld seam with relatively fine microstructure is obtained, and the mechanical properties of the joints are optimized.
- (3) It can reduce the welding deformation [20, 21]. The welding rate of LAHW increases, and the single-pass

Fig. 1 The diagram of welding defects



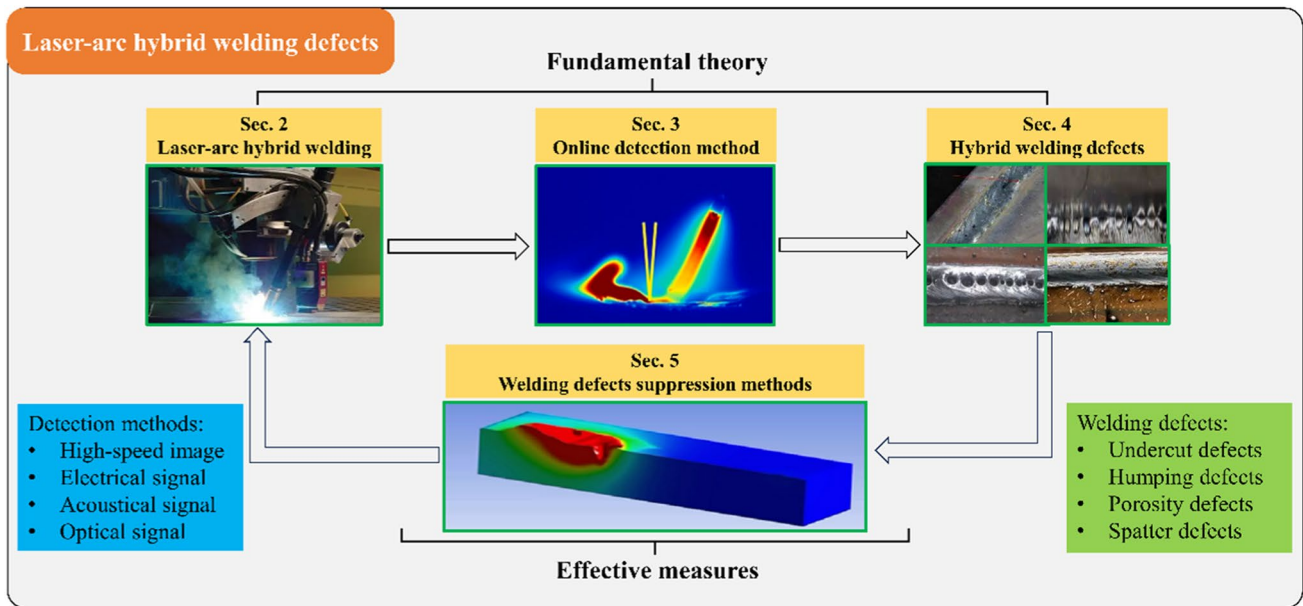


Fig. 2 The flow chart of welding defects for laser-arc hybrid welding in this review

Table 1 The comparison among arc welding, laser welding, and laser-arc hybrid welding

	Arc welding	Laser welding	Laser-arc hybrid welding
Bridging ability	Wide melting zone; good bridging ability	Narrow melting zone; poor bridging ability	Wide melting zone; good bridging ability
Residual stress and deformation	High linear energy; large residual stress and deformation	Low linear energy; small residual stress and deformation	Low linear energy; small residual stress and deformation
Productivity efficiency	High welding speed; low productivity efficiency	High welding speed; high productivity efficiency	High welding speed; high productivity efficiency
Crack tendency	High tendency for solidification	Increased crack tendency	Low crack tendency
Cooling rate	Low cooling speed	High cooling speed	High cooling speed
Penetration depth	Small penetration depth	Large penetration depth	Large penetration depth

welding wire metal deposition amount is reasonable, which avoids excessive welding heat input. The size of the heat-affected zone (HAZ) can be reasonably adjusted to decrease the local residual stress peak value.

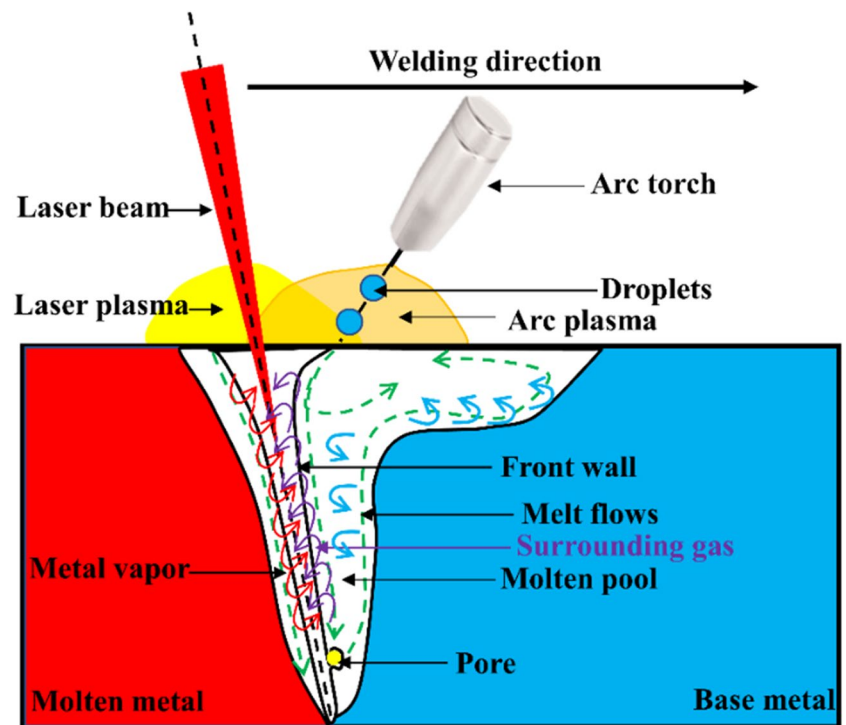
- (4) It can increase penetration depth [22, 23]. Since LAHW has two independent welding heat sources, the arc welding current, voltage and laser power can be adjusted separately to obtain different weld depth–width ratios. Meanwhile, compared to single laser self-fusion welding, hybrid welding has a filler metal, which makes the weld formation full.
- (5) It can improve welding adaptability [24–28]. Since LAHW has the characteristics of the greater filling capacity of arc welding, the tolerance of the welding gap can be increased. At the same time, by adjusting the arc welding current, voltage, and laser power separately, the joint structure with different depth–width ratios can be realized. The welding process can be car-

ried out at a higher welding speed to improve production efficiency[29].

3 Welding defects online detection methods

There are multiple variables and many uncertain factors in the welding process, which obtain information directly or indirectly to reflect the welding’s stability and quality. Achieving online monitoring of welding quality has become a remarkable research hotspot in the welding industry at home and abroad. The welding process is a complex physical–chemical process under the action of electricity, light, heat, and force. It has become the key point of welding research to monitor the acoustic, optical, electrical, and other information in real-time, which establishes the relation between feature information and welding workpiece quality and restrains the generation of welding defects by adjusting

Fig. 3 The schematic diagram of the LAHW process



and optimizing welding parameters. Nowadays, the real-time monitoring technology for welding quality has made substantial progress, and the detection methods are gradually increasing, fully utilizing characteristic signals during the welding process, such as electrical signals, acoustic signals, and optical signals, as shown in Fig. 4.

3.1 High-speed image technology

High-speed image technology can clearly record the spatial and time information of transient change processes or high-speed movement processes. It is more common to use high-speed image technology to observe and study the welding process. In the LAHW process, high-speed image is often used to take pictures of droplet transfer, welding spatter, welding plasma, molten pool flow behavior, and arc morphology.

Zhang et al. [30] argued that laser energy density continuously increased with the increase of CO₂ content, and penetration depth also increased. Meanwhile, when shielding gas is 15% CO₂ + Ar and 20% CO₂ + Ar, the welding process is stable and has less spatter as shown in Fig. 5. Zhu et al. [31] investigated the impact of different heat source leading modes and energy ratios on the stability of LAHW and found that utilizing arc-leading mode could effectively alleviate fluctuations in the molten pool and achieve a complete droplet transfer process, thus reducing the number of spatters. The droplet transfer behavior reflects the stability of the LAHW process, which plays a crucial role in the weld quality [32, 33].

3.2 Electrical signal detection technology

The common electrical signals mainly include voltage signals and current signals. Electrical signals are easy to collect and have a clear physical meaning, and they are controllable variables, which directly related to the stability of the welding process. Therefore, it is considered to collect electrical signals to monitor the welding stability during the LAHW process.

Tetsui [34] collected the instantaneous values of voltage and current signals, obtained the waveform characteristics of welding parameters, and found that this waveform feature can qualitatively reflect the droplet transfer mode. Arc waveforms can not only analyze the behavior of droplets but also understand the mechanism of spatter defect generation. Similarly, welding current and arc voltage are always key factors to affect welding quality. Sheng et al. [35] investigated the effect of laser power on droplet transfer behavior and electrical signals. The droplet transfer time and current peak time were extended as the laser power increased, and the current base time was shortened. With the increasing of laser power, the droplet growth cycle was extended, and the droplet size was increased. Therefore, the waveform of the electrical signal was the main method to obtain a stable welding process, including a large amount of information about welding arc. Any slight changes in the droplet could be mirrored timely in the electrical signal waveforms, as shown in Fig. 6. Zhang et al. [36] studied droplet-transfer

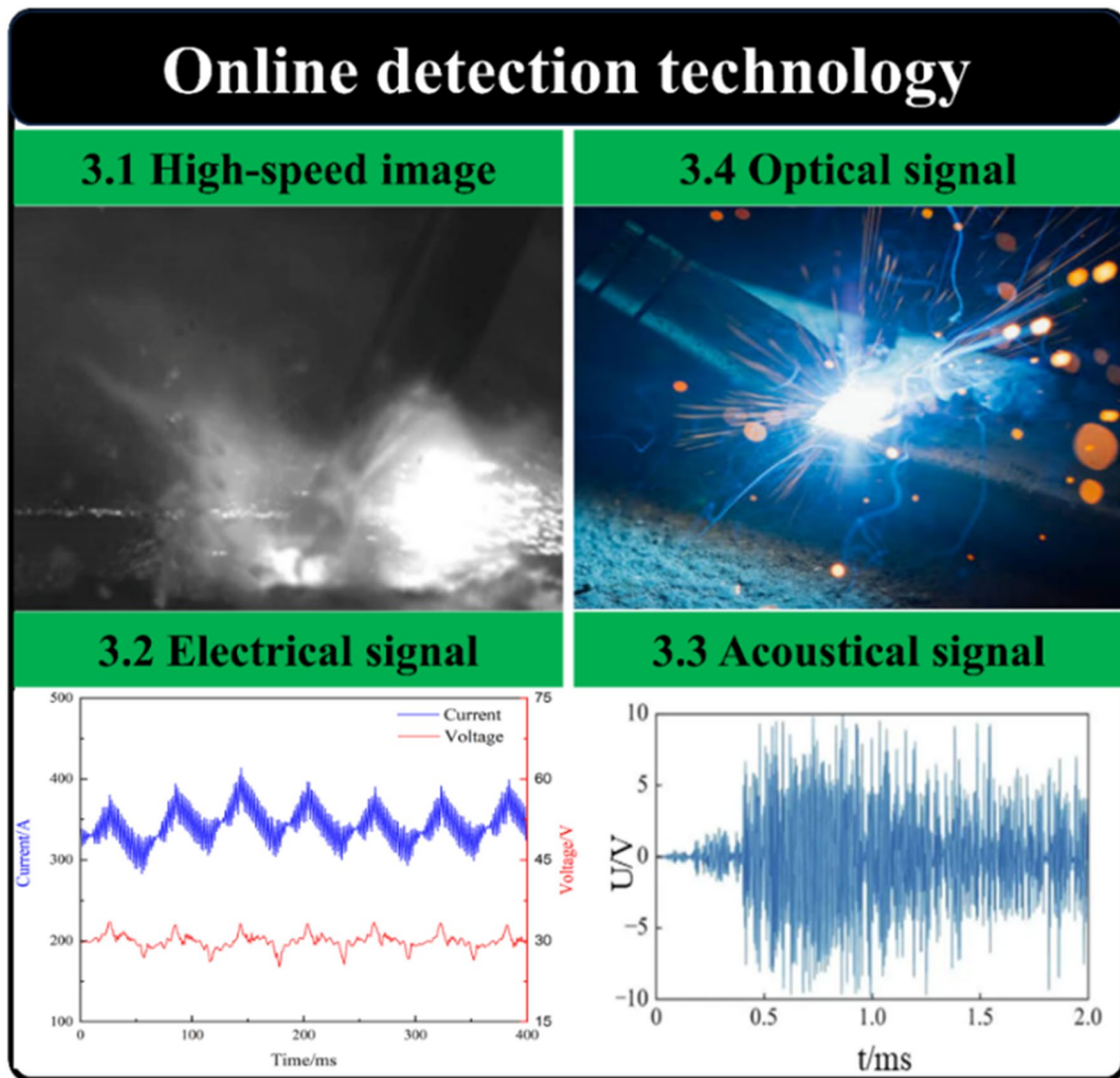


Fig. 4 Welding defects online detection technology

behavior during single-pulse MAG welding and laser-pulse MAG hybrid welding with high-speed image and electrical signal acquisition system. It could be concluded that, under the action of laser, the distribution range of welding voltage decreased, the probability density of high voltage distribution decreased, and droplet transfer became more stable.

The electrical signal device is simple to operate, and the signal is not easily disturbed by external signals. However, the number of information contained in the electrical signal is relatively less, which cannot fully reflect the complex dynamic changes in the welding process. Moreover, the monitoring feedback time of the electrical signal system is relatively short, and the sensitivity is low, greatly limiting its application in the real-time monitoring process.

3.3 Acoustical signal detection technology

The acoustic signal is also a useful signal in the monitor process. In arc welding, the random non-stationary signals generated by the arc combustion process often contain dynamic changes. The skilled welding engineer can judge the welding process stability, welding spatter situation, and droplet transfer mode based on the arc sound signal, in order to achieve the goal of improving welding quality. There are many related research reports in this field at home and abroad.

Račko [37] associated ultrasonic signals with welding crack propagation in the welds based on a typical stress theory model and compared the predicted acoustic emission signal with the actual measured acoustic signal values, thus proposing a welding crack propagation criterion. Grad et al. [38] collected acoustic signals

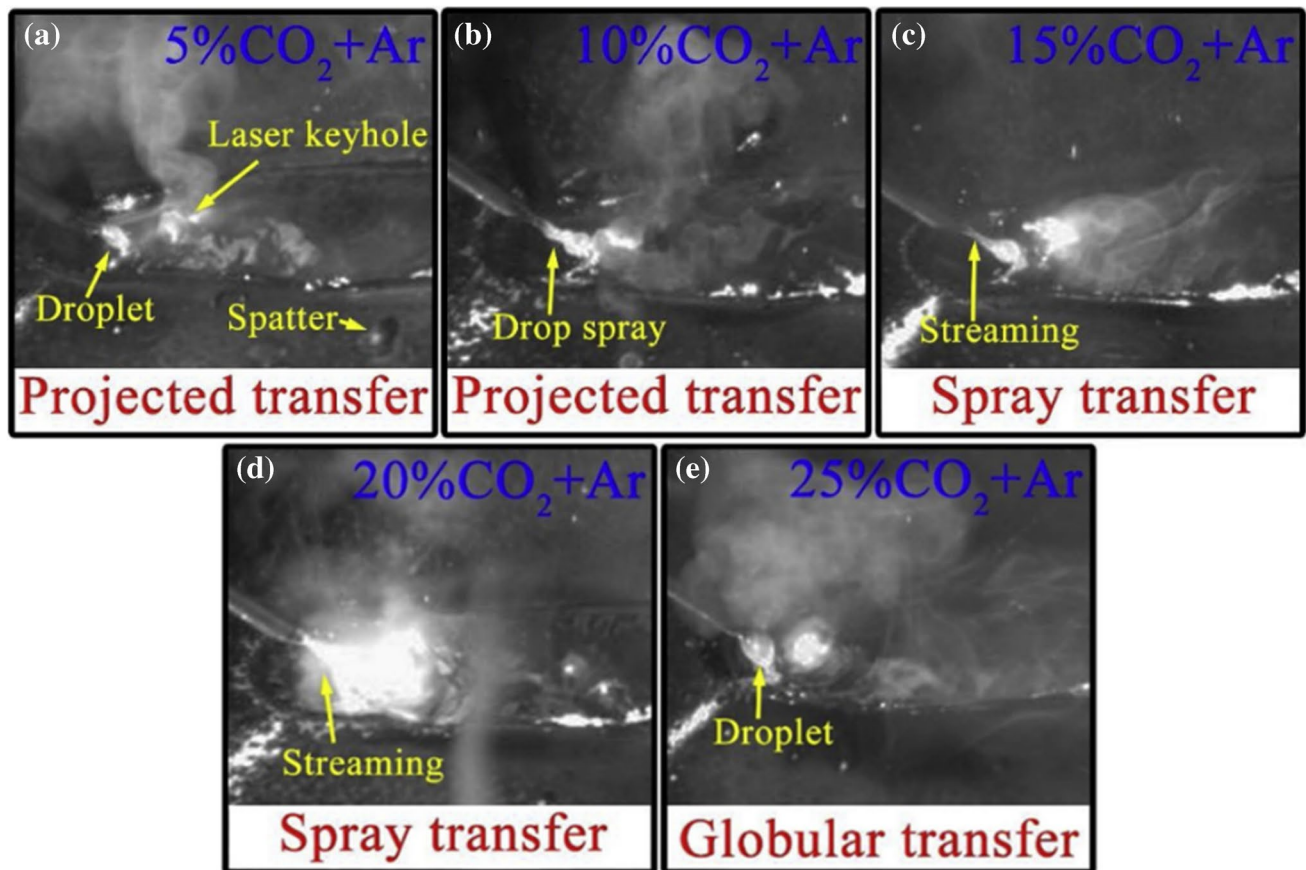


Fig. 5 High-speed camera images observing the metal transfer behaviors during the HLAW process with different CO₂ contents [30]

and explored the feasibility of using acoustic signals for real-time monitoring. It was found that the frequency of the acoustic signals was related to welding stability, and the type of shielding gas had a significant impact on the acoustic signals.

However, due to the complex and difficult separation of acoustic signals, the droplet transfer, the release of internal tension, the shielding gas flow rate, and the flow of the molten pool can all generate sound. The acoustical signal is also susceptible to interference from other factors, such as the external environment, which affects measurement accuracy. These factors make it difficult to establish a definitive relation among acoustical signals, welding stability, and welding quality, which greatly limits the application of acoustical signals in actual production. At present, the industrial application of real-time monitoring of the welding process with acoustic signals has not been publicly reported.

3.4 Optical signal detection technology

The optical signal is the light radiation emitted by high-temperature plasma. The plasma light radiation signal

which monitors can reflect the absorption degree of the laser by the workpiece during the welding process. The most commonly used sensing signal is laser-induced plasma light radiation. The interaction between the heat source and plasma directly affects the welding process. Therefore, the fluctuation of plasma is a direct reflection of the dynamic changes. Online monitoring can be achieved by observing plasma. The radiation generated by plasma mainly includes reverse bremsstrahlung radiation, hot electron radiation, and photoelectron radiation.

The first two kinds of radiation produce a continuous spectrum, and the last kind of radiation produces a line spectrum, whose spectral lines are mainly distributed in the visible blue light range. By measuring the absolute intensity, relative intensity, and contour of radiation spectral lines, physical parameters such as emission coefficient, plasma temperature, and electron density in plasma are determined. This analysis method is called spectral analysis. As spectral measurement is a non-contact measurement method that does not affect the light source, the measurement is accurate and stable, and it is the most commonly used research method for plasma radiation analysis in the domestic and overseas.

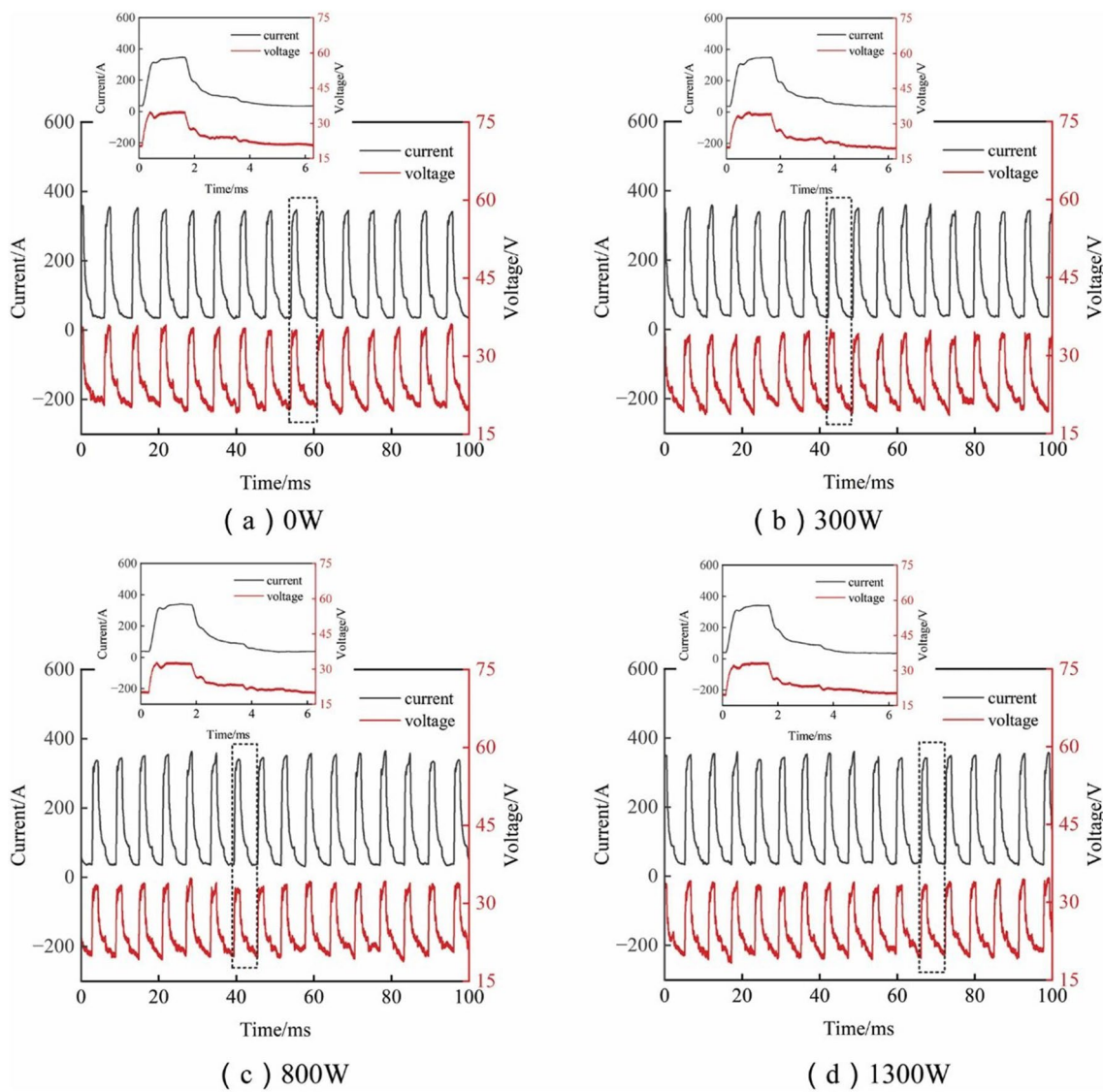


Fig. 6 Welding current waveform under different laser powers [35]

4 Laser-arc hybrid welding defects

The strong coupling effect of LAHW heat sources and the difficulty in optimizing and controlling numerous process parameters result in the generation of welding defects, which seriously affect the welding joints' quality, as shown in Fig. 7. Therefore, this review elaborates on the formation mechanism and forming process of major welding defects, such as undercut, humping, porosity, and spatter defects.

4.1 Undercut defects

The undercut is the welding defect formed by incomplete coverage of the deposited metal on the workpiece along the weld toe. As shown in Fig. 8, undercut defects can be divided

into three types: curved, crack-like, and micro-flaw types [39]. It is a serious surface defect, which can cause stress concentration and welding crack easily. The undercuts will decrease the mechanical properties of the welds. If not kept at a minimum value, the undercuts will severely reduce the fatigue performance of the whole welded structure [40–43].

The formation of undercut defects is in close contact with the tension of the solid, liquid, and gas phases at the edge of the molten pool. Without considering the condition of arc force and molten pool flow condition, from the perspective of statics, the stress state of welding can be analyzed through the two-dimension model, as shown in Fig. 9. Equation (1) at the junction of solid, liquid, and gas is [44]:

$$S = S_{sg} - (S_{sl} + S_{gl} \cos \theta) \tag{1}$$

Fig. 7 The common welding defects in this review

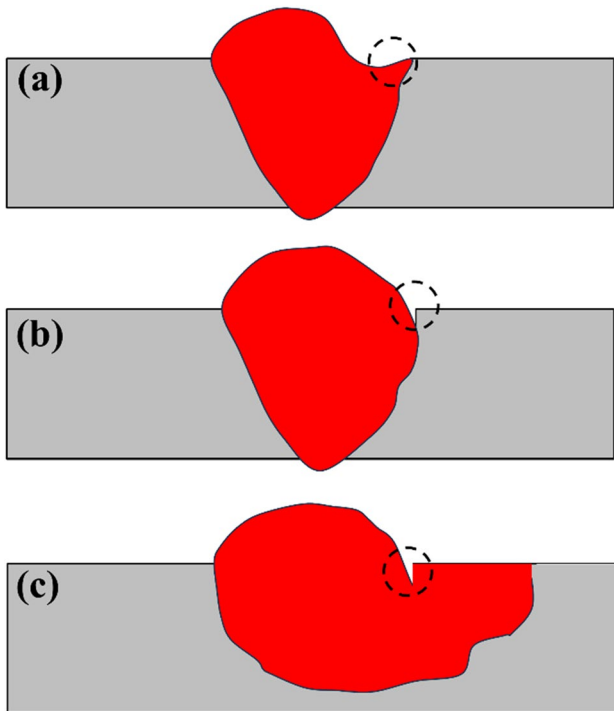
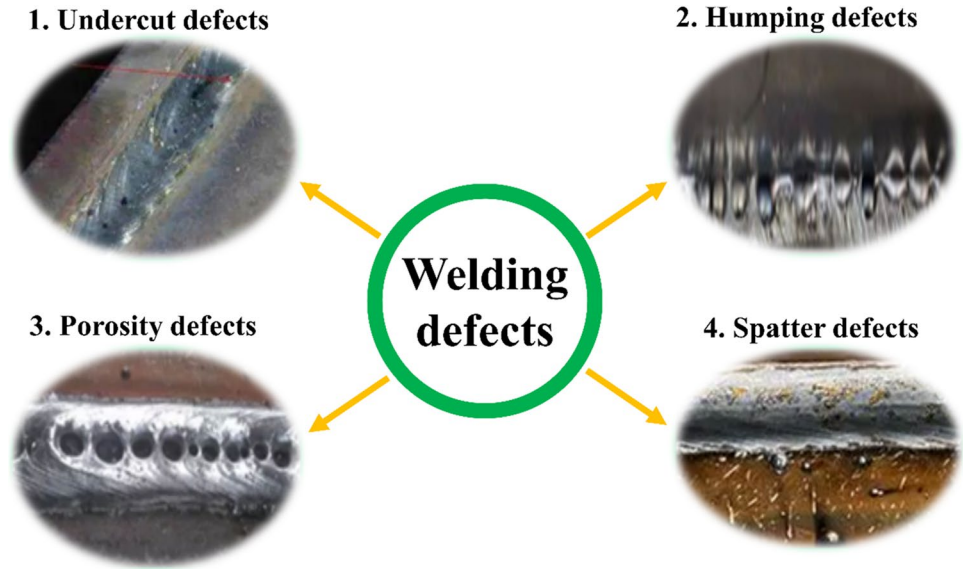


Fig. 8 The type of undercuts at the weld toe of butt joints: **a** curved, **b** crack-like, and **c** micro-flaw

where θ is the contact angle of the solid-liquid interface, S_{sg} is the solid-gas surface tension coefficient, S_{sl} is the solid-liquid surface tension coefficient, and S_{gl} is the gas-liquid surface tension coefficient. It can be found in Eq. (1) that when $S = 0$, the combined force is just in balance. It is a critical situation where undercuts do not occur. When $S > 0$, the combined force points towards the outside of the molten pool

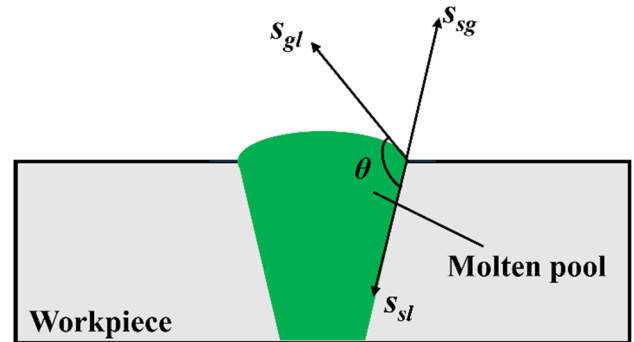


Fig 9 Schematic diagram of the surface tension of the triphase of the molten pool cross-section

without undercut defects, and the liquid metal spreads out. When $S < 0$, the combined force points toward the interior of the molten pool, and the liquid metal will shrink. The molten metal will gather inward and form undercut defects. According to the above theory, the measures which reduce the tendency of undercut defects are to decrease the contact angle and weld width and increase the deposited metal amount. The contact angle mainly depends on the material composition, gas composition, interface state, and cooling conditions.

At present, researches on the generation mechanism of undercut defects mainly focus on the following three aspects, as shown in Fig. 10. Firstly, from the molten pool force state, it is thought that the change in the direction and size of the force will cause the formation of undercuts. Secondly, from the molten pool flow state, it is argued that the molten pool flow behavior is the key factor for the occurrence of undercuts. Finally, from the numerical simulation research, the coupling of arc force and temperature field is used to analyze the reasons for undercut generation.

Firstly, from the perspective of the molten pool force state, it can be observed that undercut defects are in close relation to force condition. Mendez et al. [45] developed a numerical model, analyzing the balance of gravity, surface tension, and arc pressure in the molten pool. They found that the force acting on the molten metal surface could cause undercut defects. Meng et al. [46] observed that arc shear force would lead to undercut defects. Hu et al. [47] found that the gravity component of liquid metal along the welding direction was increased by specific angles of welding, which could be helpful to the transverse spreading of molten metal. Therefore, the flow rate of the molten pool decreased as the workpieces' inclination angle increased. Gao et al. [48] changed the workpieces' inclination angle to prevent undercut defects, as shown in Fig. 11. It was found that undercuts could be improved perfectly when the workpieces' inclination angle was 30°, and it had a close connection with the molten metal flow.

The welding speed could influence the molten pool force state. The undercut is quite common in high-speed welding, and it is difficult to overcome in high-speed welding [49]. The welding speed is usually closely related to the occurrence of undercut defects [50]. When the flow rate of liquid metal exceeded 0.4 m/min, the transverse transfer of molten metal was insufficient, which caused undercut defects [51]. The formation of undercut defects is caused by melt body flow solidification, which is relevant to viscosity and surface tension. With the increase in temperature, the surface tension will decrease, which could have a negative impact on the adhesion of solid materials and could lead to undercut defects, possibly [52]. With the continuous increase in welding speed, the undercut defects have gradually become a serious problem [53]. Similarly, the coupling of welding speed and high laser power could further cause welding defects [54]. Alam et al. [55] argued that the molten pool

Fig. 10 The generation mechanism of undercut defects in this review

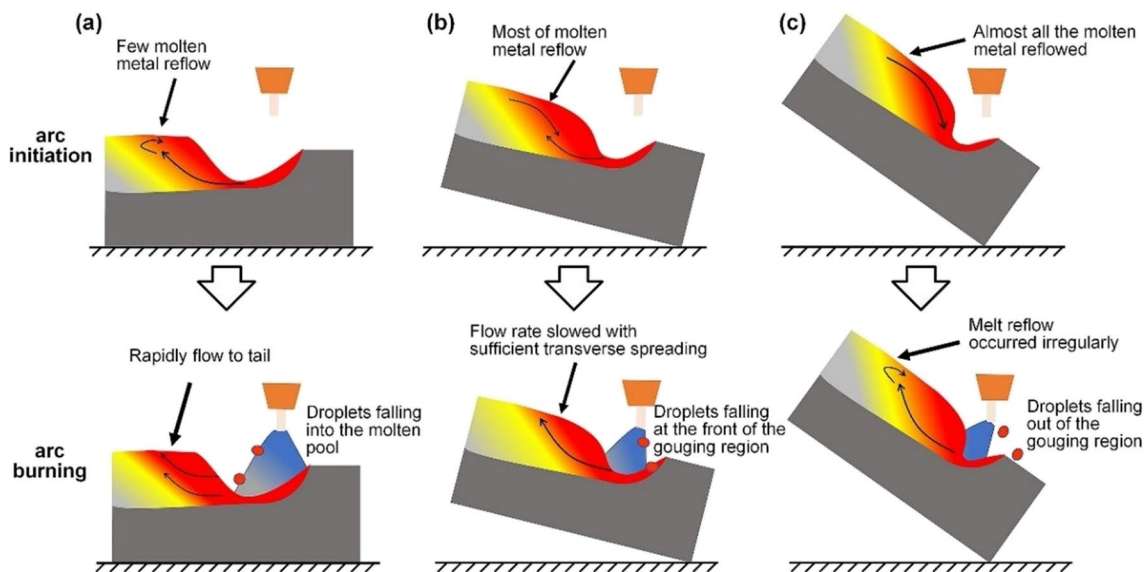
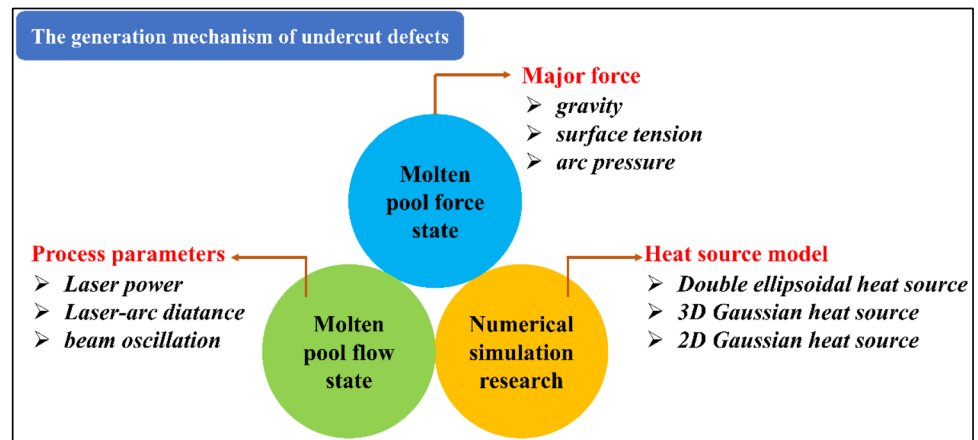


Fig. 11 The schematic of melt flow at varied inclination angles: **a** 0° (Few molten metal reflow), **b** 30° (Most of molten metal reflow), and **c** 40° (Almost all the molten metal reflow) [48]

was elongated at higher welding speed, and the molten metal on the side wall flowed towards the center, which resulted in undercut defects, as shown in Fig. 12.

The existence of the thin oxide layer on the workpiece surface will make the arc contract, increase arc pressure, and have a low oxide density. During the welding process, it is easy for the oxide to reach the edge of the arc crater area and solidify rapidly under the action of the molten pool oscillation, which hinders the further transverse spreading of the molten metal, results in insufficient molten metal filling at the edge of welds, and generates deeper sharp corner undercut defects. Karlsson et al. [56] studied the formation mechanism of undercut defects under two conditions: retaining surface oxides or removing surface oxides, as shown in Fig. 13. The research suggested that the steel surface with mill scale could produce sharp undercuts and form sharp oxide inclusions at the weld edge. The presence of oxides constrained the arc and increased the arc force, which resulted in greater impact force and deeper grooves. At the same time, the density of oxides was smaller than that of the molten metal, which was pushed to the edge of the molten pool. During the solidification process, the melting point was higher than that of steel, which hindered the wetting and spreading of the molten metal and generated undercut defects. Proper protection of the molten pool could reduce the occurrence of welding defects. Oxides usually cause undercut defects. Norman et al. [56, 57] found that the oxides that entered into the molten pool would probably arrive at the edge of the arc crater. The molten metal would solidify quickly when the temperature dropped. The reason for the generation of undercuts was the transverse spreading of molten metal was restrained. Nguyen et al. [39] found that the occurrence of undercut defects was obvious when joining the workpieces with an oxide layer and caused larger welding defects and

poorer fatigue performance. Therefore, removing the surface oxide film before welding would eliminate oxide inclusions and form a smooth surface.

Secondly, from the perspective of the molten pool flow state, it can be found that the molten pool flow condition has a close connection with undercut defects. Frostevarg et al. [58] suppressed the generation of undercut defects by adjusting the D_{LA} (distance between laser and arc) and changing the geometric conditions of the melt flow. According to the high-speed image, it could be seen that the keyhole and the position of the keyhole had an impact on the molten pool flow. If the D_{LA} was quite large or small, the undercut defects would occur. When the laser keyhole was adjusted to the transition area between the arc groove and the molten pool, the undercut defects were suppressed. The asymmetry between the arc and laser exacerbated the formation of undercut defects, which was usually caused by the narrowing of the melt flow behind the groove. Eriksson et al. [59] studied the molten pool flow behavior and generation of undercut defects through high-speed image and Particle Image Velocimetry algorithms. With the increase in laser power, the inclination angle at the interface between the fusion zone and the edge of the base metal increased. The reason for this phenomenon was that the fluidity of the molten metal on the inner wall and front edge of the keyhole was enhanced. Hao et al. [60] investigated the effect of circular beam oscillation on the flow behavior of the molten pool and found that the circular beam could change the molten pool flow behavior. With the increase in scanning frequency and amplitude, the width and length of the molten pool increased, and the transition at the tail of the molten pool became smooth, which was conducive to the flow of molten metal from the center of welds to both sides of welds. Li et al. [61] investigated the molten pool flow behavior of beam oscillation and the

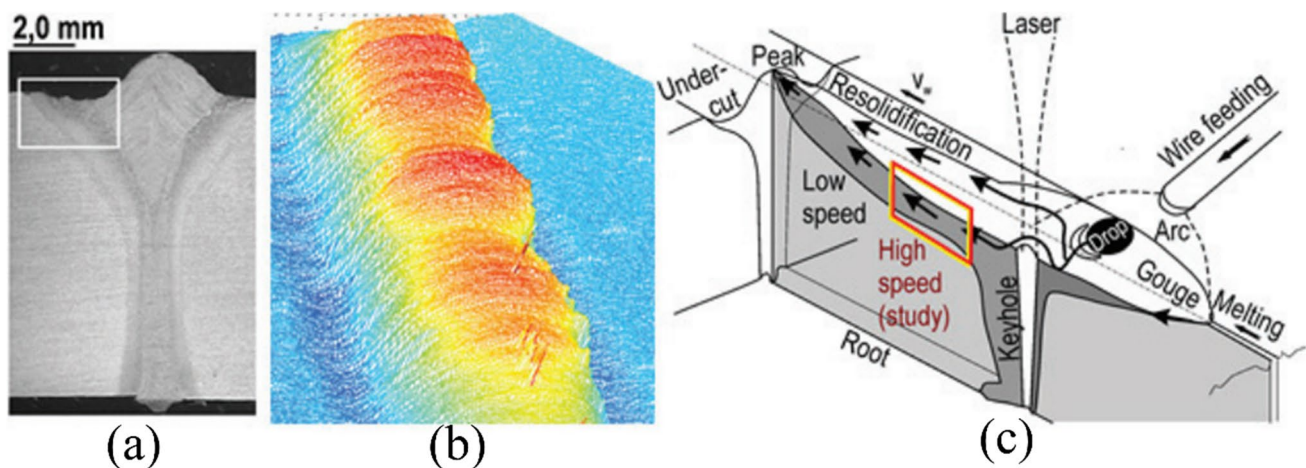


Fig. 12 The generation of undercut defects: **a** the weld cross-section of undercut, **b** scanned weld surface topology, and **c** sketch of hybrid welding under high speed [55]

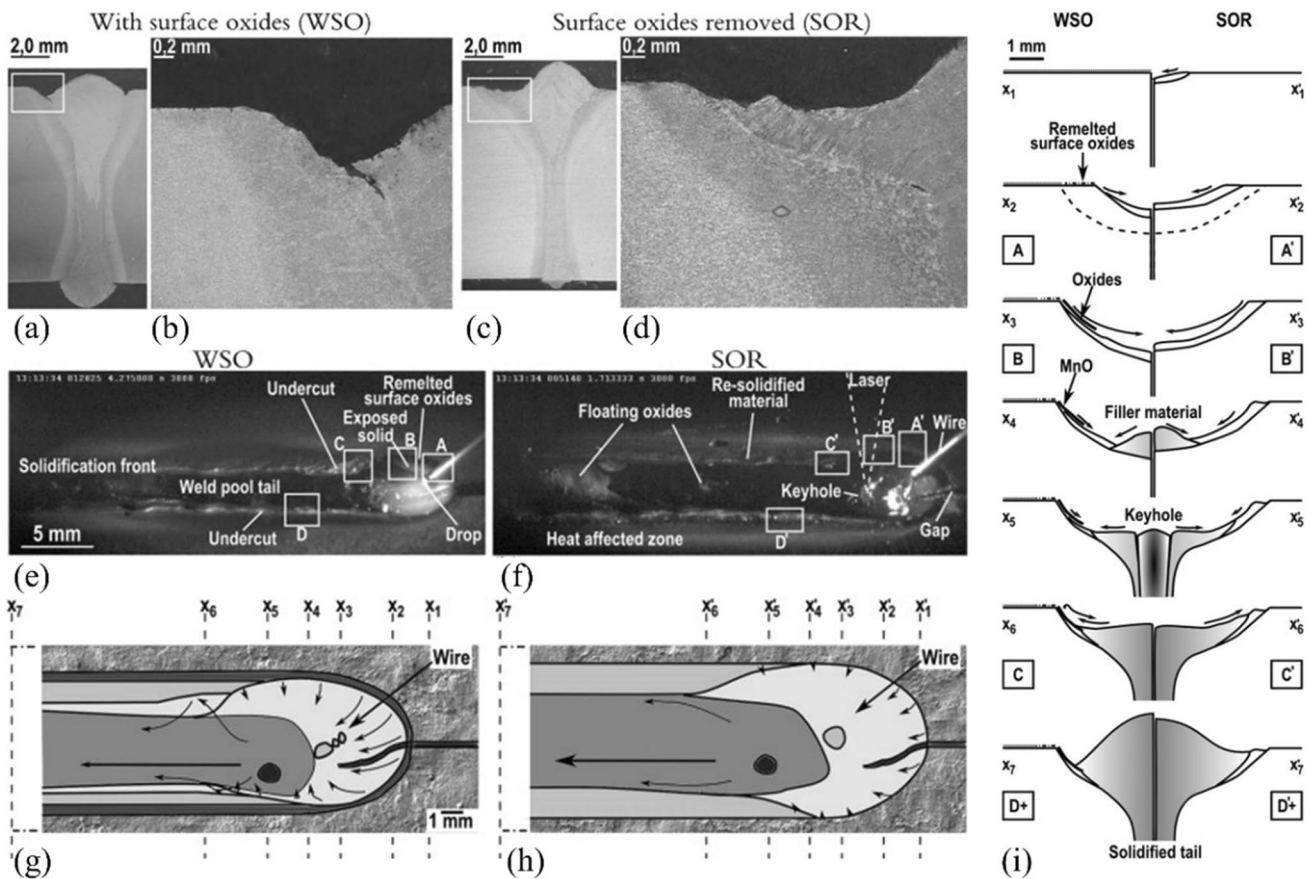


Fig. 13 Formation mechanism of the undercut under the condition of keeping the rolling state or removing the oxide: **a** and **b** with surface oxide cross-section, **c** and **d** without surface oxide cross-section, **e**

and **f** high-speed photographic image with/without surface oxide, **g** and **h** corresponding schematic diagrams, and **i** solidification process schematic diagram [56]

influence of laser beam oscillation parameters on weld formation and welding defects. When beam oscillation was not added, serious undercut defects appeared in front of the welding joint. After adding beam oscillation, the undercut defects on the front wall were suppressed, and the downward flow of the liquid metal at the rear of the molten pool was improved. In addition, the microstructure of the welds was refined and the mechanical properties were improved. Tao et al. [62] carried out research on LAHW of pipeline steel, it could be found that from the high-speed image, stable arc characteristics and smooth molten pool were formed when laser power was 400 W. The optimal weld was obtained without undercut defects.

In addition, there is a strong fluidity of molten metal driven by surface tension. On the one hand, the molten metal can spread towards the edge of the welds along the welding direction, which prevents the formation of undercut defects. However, for single-arc welding, when the welding speed is quite high, the liquid metal solidifies rapidly, which lacks sufficient time to flow to the weld toe zone and fill the gap between base metal and deposited metal. Therefore, it is

easy to generate undercut defects. After the addition of laser energy, the heat input energy increases. At a higher welding speed, the solidification rate of molten metal decreases, which has more time to flow into the weld toe zone. On the other hand, the temperature of the metal plasma inside the laser keyhole can reach up to 20,000 °K. Its temperature is far higher than conventional MIG welding. It can be observed that the hybrid welding has a higher temperature gradient. This means that the surface tension gradient inside the molten pool is greater, and the molten metal has a faster flow rate. The molten welding wire metal can flow along the molten pool and fill the weld toe in a shorter time to suppress undercut defects. Gao et al. [17] conducted research on LAHW of Mg alloy and found that the optimized LAHW process parameters could suppress the undercut defects. At the same time, the tensile strength was also improved. The undercut defects were generated due to the evaporation and loss of alloy elements, and it could be improved by increasing the wire feed speed in LAHW.

Finally, from the perspective of numerical simulation research, it can be observed that numerical simulation

researches could analyze the generation mechanism of the undercut defects. Ai et al. [63] established a finite element numerical model for the keyhole morphology and molten pool fluidity during high-speed welding, which verified the Rayleigh instability of the molten pool. The results showed that the Rayleigh instability caused by the increase in the length of the molten pool is the primary element, which led to the instability of the molten pool's dynamic behavior, as shown in Fig. 14. Zhou et al. [64] simulated the transient keyhole dynamics, obtaining the interaction mechanism between the liquid droplets and molten pool and clarified the shape and composition of solidified weld seams. Liu et al. [65] analyzed that the formation of undercut defects had relations with the welding arc and molten pool flow behavior through experiments and simulations. By observing the flow process of the molten pool, it could be seen that there were effects of multiple forces, such as Lorentz force, electromagnetic force, and arc force. The liquid metal was subjected to a combination of plasma drag force, droplet impact force, and arc force, which flowed toward the rear area of the molten pool. In the meantime, the arc root hindered the flow and diffusion of liquid metal. Therefore, there was only a thin layer of liquid below the arc. As the arc struck, the thin liquid layer solidified rapidly due to the excessive cooling rate, which caused the generation of undercut defects, as shown in Fig. 15. Mendez and Eagar [52] proposed a model for predicting weld solidification. High arc pressure pushed molten metal towards the back of the molten pool, forming a thin liquid metal film that came into contact with solid base metal. Premature solidification of this thin layer would inhibit wetting on both sides of the welds, which caused the formation of undercuts. However, Nguyen et al. [53] emphasized only the thin layer at the front, the vital effect of the molten pool

edge in transferring molten metal to the trailing edge was ignored. Although some theories simulated molten pool flow, the reason and physical mechanism that generated undercuts were still unknown. Nevertheless, some technological methods have been proved to be efficient in restraining undercut defects by slowing down the backflow of molten metal.

There are two different methods for suppressing undercut defects in LAHW. First, under the interaction of laser and arc, the arc is compressed and more stable, which increases the welding wire deposition amount indirectly and improves energy utilization efficiency. The surface tension of the solid, liquid, and gas phases at the weld toe was changed, and the formation of undercuts was suppressed. Second, through the interaction of laser-arc heat hybrid sources and the mutual superposition of the two heat sources in the molten pool, the surface tension gradient inside the molten pool increases, the flow rate accelerates, and the time at which weld metal flows from the center of the molten pool to the edge of the welds is more sufficient. Ultimately, more molten metal is moved to the weld toe, which fills the weld toe and eliminates undercut defects. Furthermore, adding active agents to the welds' surface can also reduce the depth of undercut defects, such as TiO_2 and Cr_2O_3 . Since the addition of active agents reduces the surface tension of the molten metal, improving its flow-ability and spread-ability. Therefore, the combined effect of them reduces the depth of the undercut defects.

4.2 Humping defects

The humping defect refers to the regular and periodic local swelling (wave peak) and collapse (wave trough) formation of weld metal along the welding direction. The humping defect

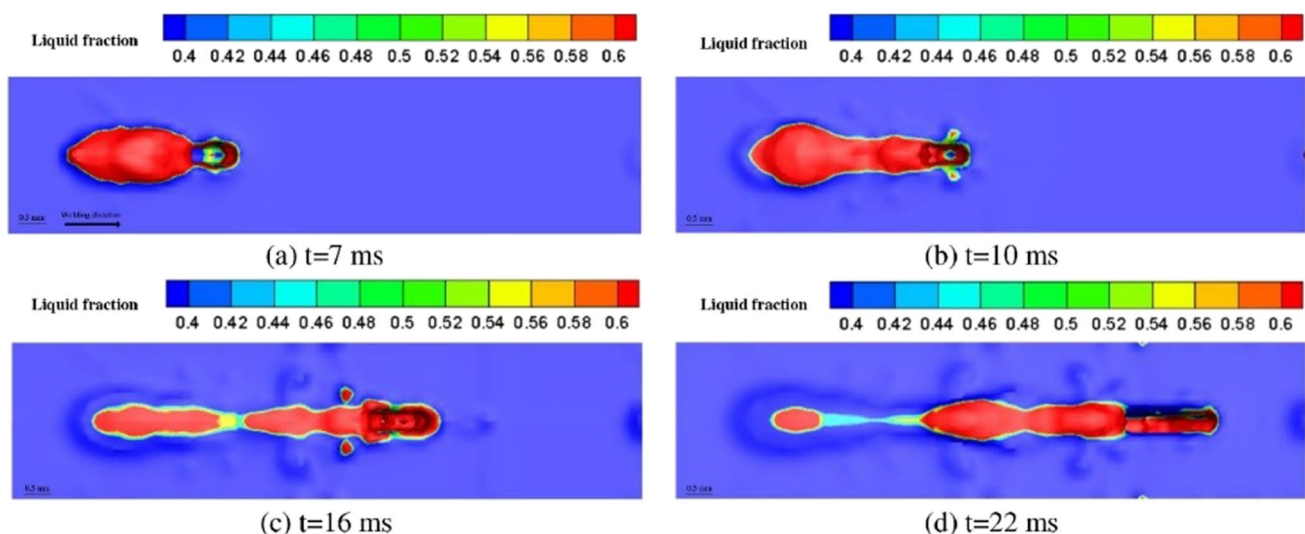


Fig. 14 The variation of molten pool morphology in the horizontal direction [63]

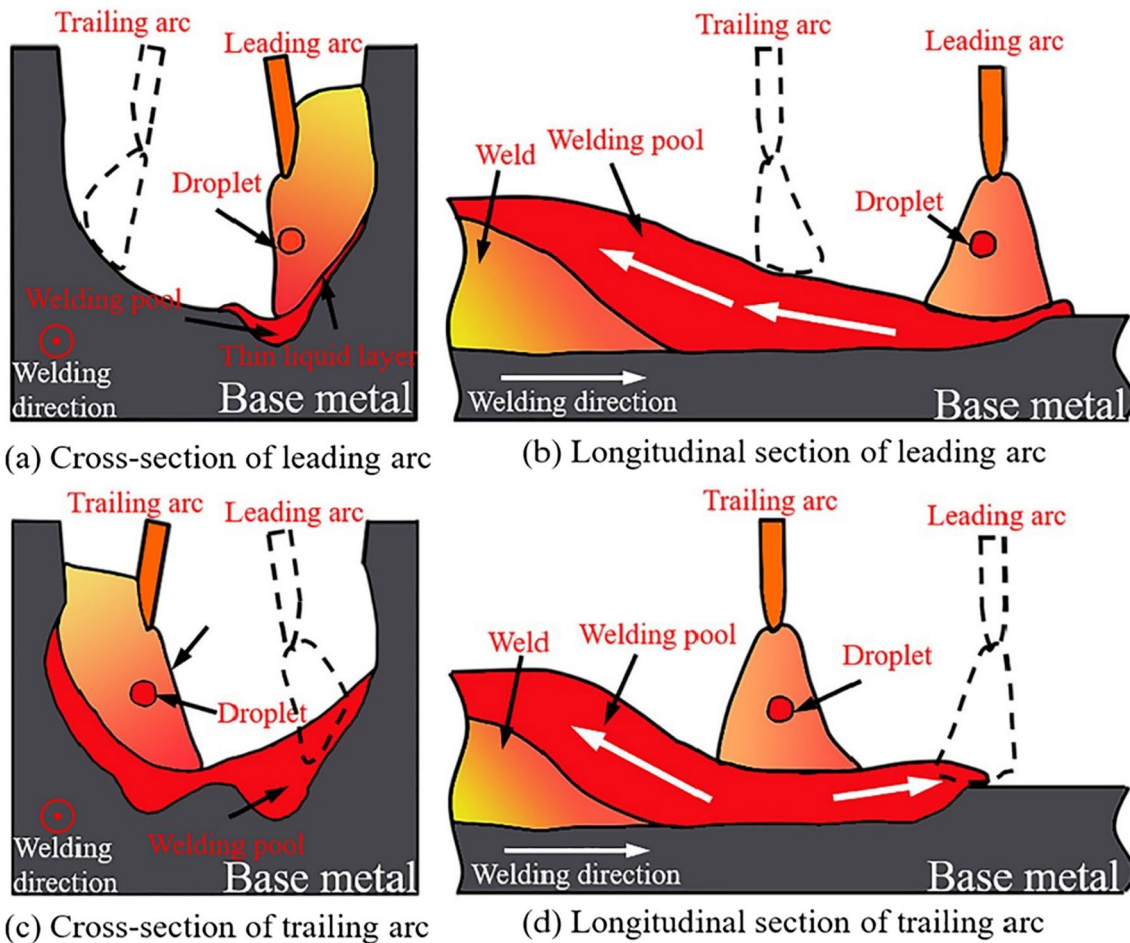


Fig. 15 Arc behavior and molten metal flow when the undercutting defect forms [65]

seriously affects the welding joint quality. Surface humping primarily exists in thin-plate welding and high-speed welding, while the generation of root humping defects mainly occurs in medium- and thick-plate welding, as shown in Fig. 16. The fundamental reason for the appearance of humping defects is the combined action of gravity and surface tension. Under the constraint of surface tension, the reflux velocity of metal droplets decreases, and the liquid metal continues to accumulate in the humping area. As the heat source moves and the welds solidify, it hinders the further growth of the humping. Finally, under the balance of surface tension and gravity, it solidifies into humping defects.

The formation mechanism of surface humping is widely recognized by the theory of molten pool wall flow, as shown in Fig. 17. In high-speed LAHW, there is a rapid wall flow inside the molten pool that flows towards the end of the molten pool, which accumulates to form a tail protrusion area. Due to the large momentum of the wall flow, it can overcome the static pressure and surface tension of molten metal at the end of welds, which causes the humping area to

grow continually. In addition, the molten metal accumulated at the end of the molten pool has a high enthalpy, which prevents the tail protrusion zone from solidifying fully. As the arc moves forward, the flow area on the molten pool wall continues to elongate as a channel for the backward flow of liquid metal. Due to the area with a thin liquid metal layer, the sectional wall flow that detaches from the arc heat effect solidifies to form a collapse due to lack of heat energy, while the tail protrusion zone solidifies to form a humping defect subsequently [66].

The humping of welds appeared on the upper surface in the arc welding first. Nguyen et al. [67] utilized high-speed images to observe the humping on the upper surface of the welds during high-speed GMAW welding. The scholar proposed that the welding speed, welding material type, and wire feeding speed were key process parameters that affect surface humping defects. The problem of humping defects also exists on the upper surface in the laser welding. Eriksson et al. [68] utilized high-speed images to capture the formation of humping defects in laser welding with high speed

Fig. 16 The schematic diagram of humping defects

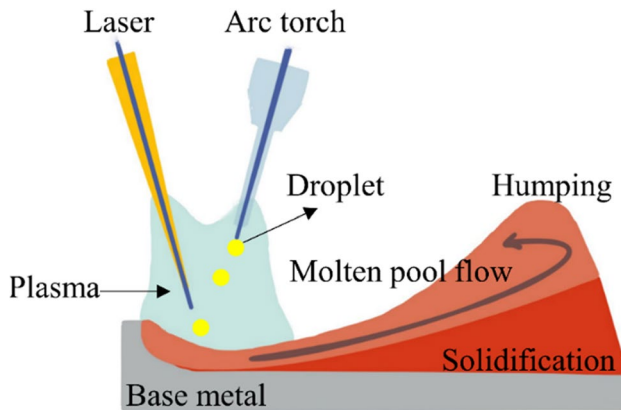
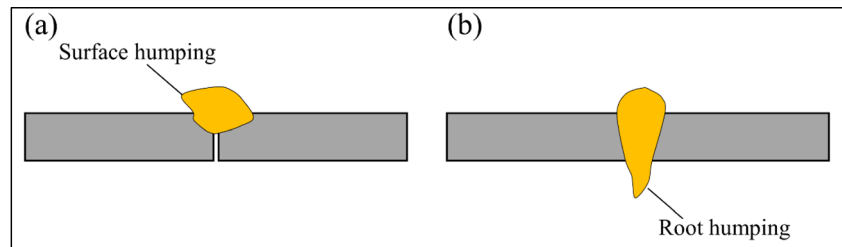


Fig. 17 The theoretical schematic diagram of surface humping

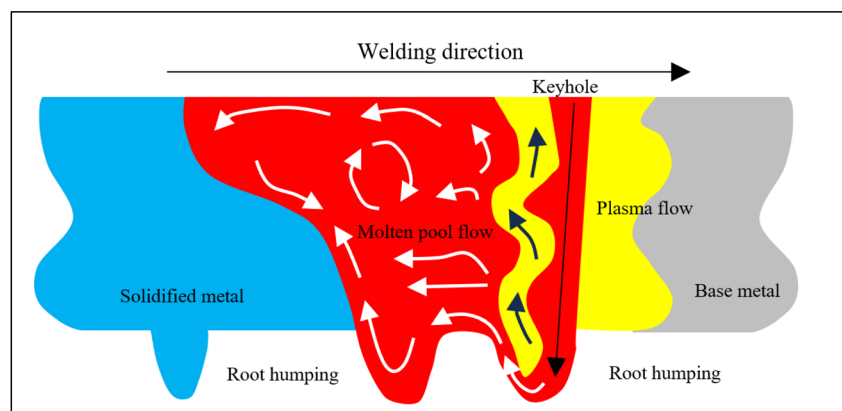
(the welding speed is more than 100 mm/s) and initially proposed the problem of surface humping in laser welding.

The above researches have all focused on the surface humping defects, but humping defects issues also exist at the welds' root. The formation of the root humping is shown in Fig. 18. In LAHW process, the inner hole wall of the keyhole is full of wrinkles, and the swelling of the keyhole wall moves rapidly towards the bottom of the molten pool under the effect of the metal vapor reaction force. Under the combined action of gravity and surface tension, the liquid metal forms multiple contoured droplets at the bottom of the molten pool. The formation mechanism of the root humping is caused by the force imbalance of the molten pool at the bottom of the welds, and the molten metal pushed out from

the deep penetration keyhole. However, the internal molten pool is difficult to observe and the interaction between laser and arc heat source is complex. How to alleviate the problem of the force imbalance of the molten pool at the bottom of the welds has not been solved. Therefore, in order to achieve the application of single-sided LAHW technology for medium and thick plates, it is necessary to study the suppression of root humping defects. At the same time, due to the large temperature difference between the front and rear edges of the bottom droplets, the reflux speed of the metal droplet decreases, which causes the molten metal volume to increase continually. With the heat source movement and the metal solidification at the tail of the molten pool, the growth rate of the droplet gradually slows down and solidifies into a humping under the balance of surface tension and gravity. Many scholars have studied the generation mechanism of humping defects through a variety of methods, which are mainly divided into two types: firstly, observing the molten pool flow and keyhole behavior directly with the method of the high-speed image or other means. Secondly, using numerical simulation to comprehensively analyze the reasons for the formation of humping defects, combined with temperature field, flow field, mass transfer, and heat transfer.

The research on the root humping defects was first started by laser welding. Kaplan et al. [69, 70] found the root humping defects when the 16-mm stainless steel was joined with a 15-kW fiber laser. However, comparing the picture of root humping with normal welds on the surface molten pool, it was found that the appearance of the root humping was relevant to excessive heat input. The imbalance between gravity

Fig. 18 The theoretical schematic diagram of root humping



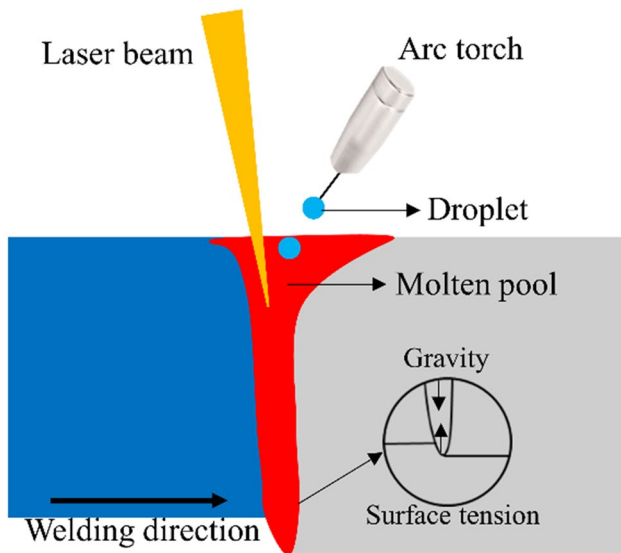


Fig. 19 The forces analysis of the bottom of the molten pool

and surface tension makes the liquid metal downflow and accumulate at the bottom of the welds, as shown in Fig. 19. After the solidification of the molten pool, the welds appear the phenomenon of upper surface collapse and root humping [71–74]. The imbalance force of root humping defects in this review is summarized in Table 2.

Jan Frostevarg [75] utilized high-speed images to study the generation mechanism of root humping. He believed that the imbalance of molten pool gravity and surface tension caused the root humping defects. With the increase in thickness of workpieces, the molten pool gravity would also increase. The surface tension at the bottom of welds was the key factor for the formation of the root humping, as shown in Fig. 20. Palmer et al. [76] established a model for a molten

pool with X-ray transmission system in LAHW. He argued that the imbalance between molten pool gravity and surface tension was the main reason for the root humping. At the same time, the effect of surface tension at the bottom of the welds on the root humping defects was studied. For the flow of molten pool in LAHW, Q Pan et al.[78] used a high-speed X-ray real-time transmission system to analyze the behavior of the deep penetration keyhole, the geometric shape of the molten pool, and the flow characteristics of molten metal inside the molten pool. It was found that a large amount of molten metal flowed out from the bottom of the keyhole, and the main reason that generated the root humping was that molten metal could not flow back timely. Based on the current research on root humping defects, the imbalance between gravity and surface tension is the direct reason to cause root humping defects. The complex movement of the molten pool in hybrid welding aggravates the imbalance. However, these factors have not been effectively combined with the process for the formation mechanism of root humping. Eriksson [77] found that humping also appeared at the welds’ root. This study confirmed that the root humping was caused by many factors, including the surface tension and gravity of the molten pool. This research considered gravity as the main factor, which meant that the root humping defects were different from the surface-humping defects.

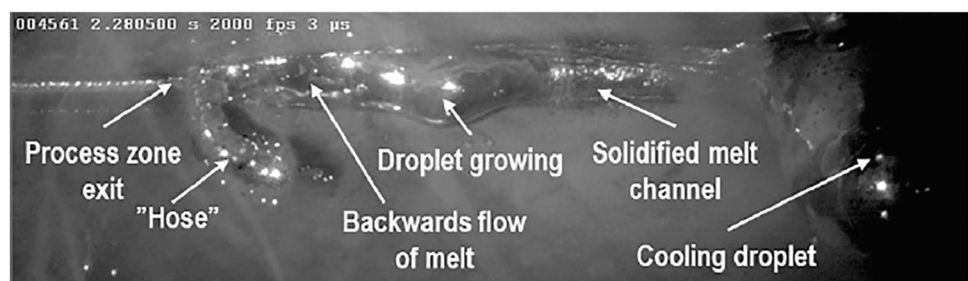
In addition, the change of welding process parameters also affects root humping defects. Different researchers have given different explanations for the influence of process parameters on root humping defects. The influential parameters are summarized in Table 3.

Zhang et al.[79] analyzed molten pool fluidity through high-speed image, and observed that the formation of root humping was related to high welding speed, which caused the molten pool flow to be more intense, thus increasing the tendency of humping defects. They also believed that there

Table 2 The imbalance force of root humping defects in this review

No.	Plate thickness	Material	Welding method	Ref.
1	12 mm	S420 MC	Laser welding/hybrid welding	[75]
2	4.8 mm	DH36 steel	Laser welding/hybrid welding	[76]
3	12 mm	High-tensile strength steel	Hybrid welding	[76]
4	8 mm	304 stainless steel	Laser welding	[77]

Fig. 20 The generation mechanism of root humping defect [75]



was an optimal welding speed range in the welding process, which could inhibit the formation of the root humping defects. The heat source leading mode has a relation with the formation of root humping in the LAHW process. Tang et al. [80] compared the arc-leading mode with the laser-leading mode and found that the arc droplet transfer had less impact on the molten pool under the arc-leading mode. Therefore, the formation of root humping was suppressed easily. Atabaki et al. [81] studied the humping defect in the LAHW. They conducted experiments from the perspective of the coupling effect between laser and arc heat source and found that there would be no humping defects at the welds' root when the D_{LA} was 8–12 mm. Pan et al. [82] utilized laser-GMAW hybrid welding with different shielding gas compositions and found that the humping defect at the root of the welds is less with the increase of CO_2 ratio. At the same time, the study suggested that the increase of oxygen content in the welds could increase the viscosity of the weld and reduce its fluidity. Haug et al. [71] analyzed the flow process of the molten pool, as shown in Fig. 21. The difference in humping defect was compared and analyzed by using a CO_2 laser and solid-state laser. It was found that the laser wavelength had a greater impact on the size of the humping shape. At the same time, it was proposed that solid-state laser was more sensitive to the humping at the welds' root. Zhang et al. [83] used a 10-kW fiber laser to join stainless

steel thick plates through laser self-fusion welding and studied the factors affecting the process parameters of the root humping defects. They argued that the focus position affected the penetration mode of laser keyhole welding and determined the formation of humping defects. At the positive defocus amount, the root humping had a large volume with periodicity, as shown in Fig. 22. At the negative defocus amount, the root humping had a small volume without obvious periodicity, as shown in Fig. 23. Furthermore, when negative defocus amount was applied, the welding speed could be optimized to control root humping defects. Finally, the application of shielding gas has played a positive role in reducing root humping defects.

With the widespread application of high-power lasers, the issue of root humping has become increasingly a focal point. Researchers have conducted research and exploration on the suppression measures for humping defects. In order to restrain the generation of root humping in LAHW. Cao et al. [84] added ceramic backing plates to the back of the welds to suppress the formation of root humping defects. Shen et al. [85] utilized laser welding to join the thick high-strength steel with the horizontal butt joint method and compared it with the flat welding process under the same process parameters. It was found that horizontal butt joint is not easy to produce humping defects. Sun et al. [86] also used the horizontal butt joint method to join a 20-mm thick 304 stainless steel, achieving the goal of suppressing humping defects. Avilov et al. [74] added an oscillating electromagnetic field at the bottom of the workpiece, it could provide an upward Lorentz force to support the internal molten pool, prevent it from falling down, suppress the occurrence of surface collapse, and suppress the generation of root humping effectively. Yamba [87] found that the collision of the molten metal caused by lateral flow towards the top plate and bottom plate, and the interruption of the flow channel in the molten pool are the reasons for the formation of the root humping. As shown in Fig. 24.

Based on the above works of literature, this review summarizes four reasons for the formation of root

Table 3 The influential parameters of root humping defects in this review

No.	Influential parameters	Author	Year/ref.
1	Welding speed	M. Zhang	2013/[79]
2	Heat source leading mode	G. Tang	2019/[80]
3	Distance between laser and arc	M. Atabaki	2014/[81]
4	Shielding gas	Q. Pan	2016/[82]
5	Laser wavelength	P. Haug	2013/[71]
6	Defocus amount	M. Zhang	2019/[83]

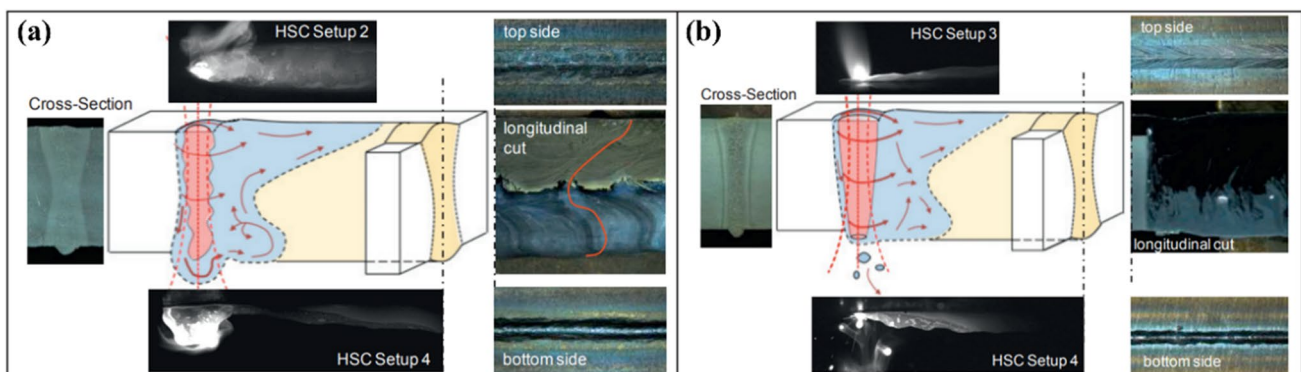


Fig. 21 The influence of different laser wavelengths on the seam quality: **a** solid-state laser and **b** CO_2 laser [71]

Fig. 22 Schematic of the formation process of humping under positive defocusing welding from a to e [83]

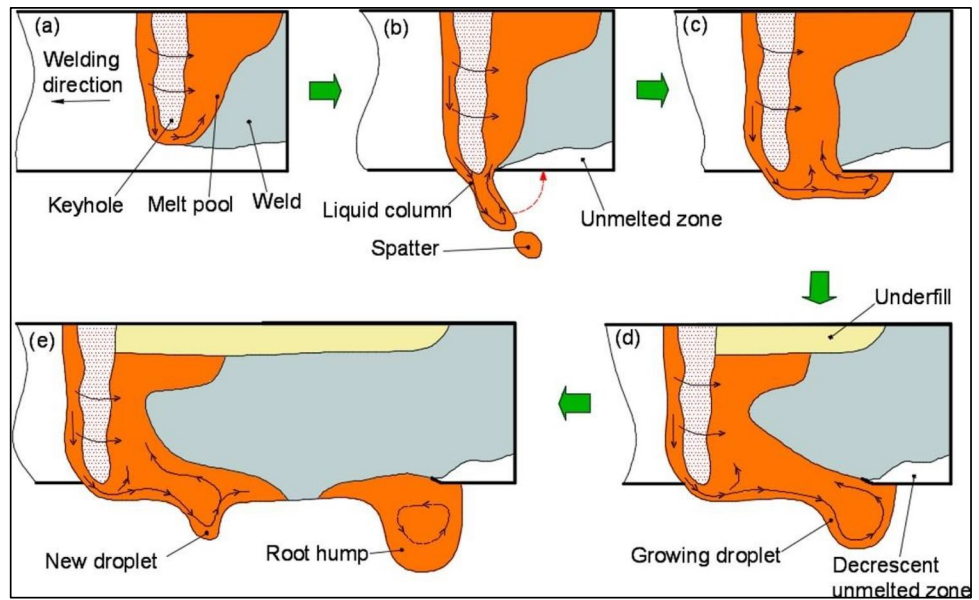
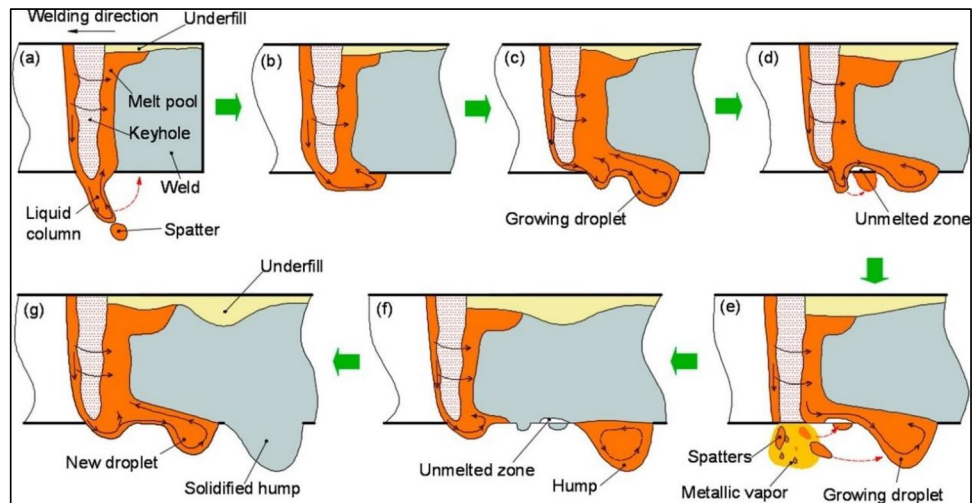


Fig. 23 Schematic of the formation process of humping under negative defocusing welding from a to g [83]



humping defects. Firstly, from the perspective of the molten pool flow rate, the root humping defects tend to form when the bottom molten pool flow rate is much higher than the welding speed. Secondly, from the perspective of force balance, the root humping was caused by the imbalance between the surface tension and gravity of the molten pool. Thirdly, from the perspective of the heat input, the excessive linear energy causes the weld to be over-penetrated and generates root humping defects. Lastly, from the interaction between laser and arc heat sources, the D_{LA} results in the formation of root humping at the bottom of the welds.

In LAHW, for the single-side welding and double-side forming on the medium and thick plates, due to the large thickness of the workpiece, the gravity of the molten pool on the bottom of welds usually makes the welds uneven,

which forms the root humping defects. At present, the existence of root humping defects seriously restricts the development and application of single-side welding and double-side forming technology. Relevant studies have shown that the formation of root humping defects becomes increasingly serious with the increase of workpiece thickness, and it is difficult to eliminate. Therefore, the suppression of root humping defects urgently needs to be solved.

4.3 Porosity defects

The porosity defects formed by the gas in the molten pool cannot escape and remain during solidification. The porosity is the most common defect in hybrid welding. In LAHW, the porosity defects mainly include three types:

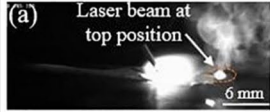
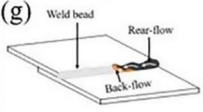
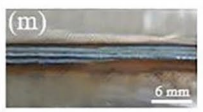
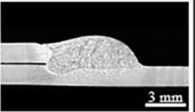
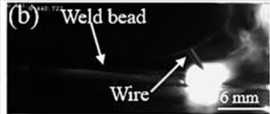
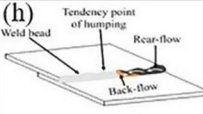
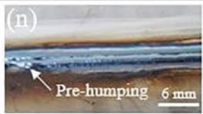
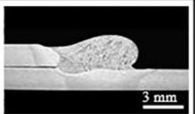
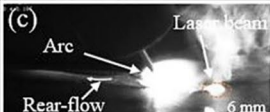
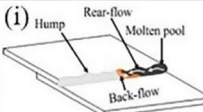
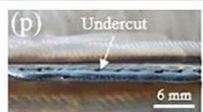
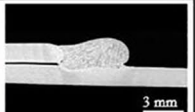
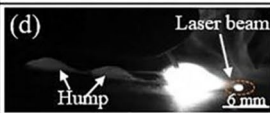
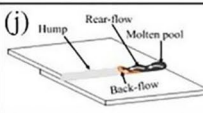
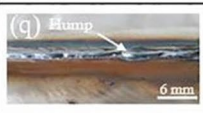
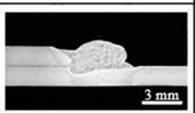
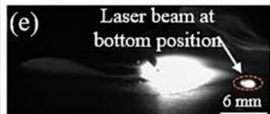
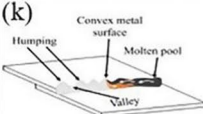

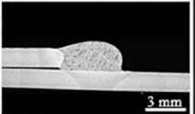
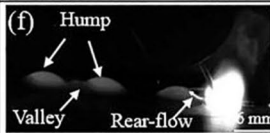
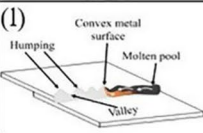
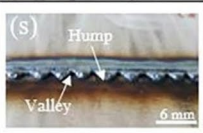
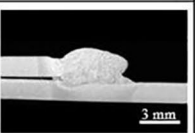
Welding parameters	Laser Pattern	High-speed image	Schematic illustration	Bead appearance	Cross-section
TS at 3.5 m/min (WFS 17.3 m/min, U 35.7 V)	Oscillated	(a) Laser beam at top position 	(g) Weld bead, Rear-flow, Back-flow 	(m) 	
	Non-oscillated	(b) Weld bead, Wire 	(h) Tendency point of humping, Rear-flow, Back-flow 	(n) Pre-humping 	
TS at 3.75 m/min (WFS 16.7 m/min, U 34 V)	Oscillated	(c) Arc, Laser beam, Rear-flow 	(i) Hump, Rear-flow, Molten pool, Back-flow 	(p) Undercut 	
	Non-oscillated	(d) Laser beam, Hump 	(j) Hump, Rear-flow, Molten pool, Back-flow 	(q) Etamp 	
TS at 4.0 m/min (WFS 20 m/min, U 36 V)	Oscillated	(e) Laser beam at bottom position 	(k) Convex metal surface, Humping, Molten pool, Valley 	(r) Hump, Valley 	
	Non-oscillated	(f) Hump, Valley, Rear-flow 	(l) Convex metal surface, Humping, Molten pool, Valley 	(s) Hump, Valley 	

Fig. 24 The influence of oscillated and non-oscillated effect on the weld bead toe angle at high traveling speed of the hybrid L-GMAW process: a–f high-speed image, g–l schematic illustration, and m–s bead appearance [87]

interlayer, hydrogen, and process porosity, as shown in Fig. 25. The interlayer porosities are large in size, irregular in shape with sharp corners, and contain black oxide substances. This is caused by the gas mixed with the flow of the refractory oxide on the workpiece surface to be welded [88]. The hydrogen porosities (metallurgical porosities) are usually circular in shape, with smooth inner walls and relatively large dimensions [89, 90]. The main reason for the formation is the decomposition and precipitation of water, moisture, and surface oil stains caused by surface contamination of the workpiece before welding, poor weld protection, etc. The process porosities (keyhole porosities) are caused by the instability of the keyhole during the welding process [91]. The keyhole is an important feature of LAHW, and its internal force balance is usually a significant factor in affecting the process porosity defects.

The porosity is one of the most common defects in the welding process. Usually, porosity defects are the main reason for workpiece failure. It will destroy the effective bearing area of weld metal and greatly reduce the mechanical properties [92] and corrosion properties of welds. It is a defect that must be strictly controlled for welding products. The fundamental reason for these phenomena is the

dynamic characteristic of laser deep penetration welding of keyhole and molten pools. Leo et al. [93] pointed out that the porosity defects inside the weld significantly reduced the tensile strength and elongation of the welding joints. Zhang et al. [94] showed that the porosity defects seriously reduced the low-cycle fatigue performance of the welding joints. Therefore, in order to reduce porosity defects and obtain high-quality hybrid welding joints, it is especially significant to clarify the influence of process parameters on porosity defects. Cho et al. [95] proved that the keyhole was prone to collapse when the base metal was aluminum alloy. The gas inside the collapsed keyhole was injected into the molten pool and became bubbles. If it did not get away from the molten pool, it would evolve into porosity defects. Ola and Doern [96] claimed that hydrogen had a higher absorption rate in liquid aluminum than in solid aluminum. It led to the formation of hydrogen porosities during the solidification process of molten metal.

Generally, there was a certain correlation between the instability of the keyhole and the fluidity of the molten metal. The interception of shielding gas, the release of super-saturation gas dissolved in the molten pool, and the evaporation of low melting point elements may lead to the formation of

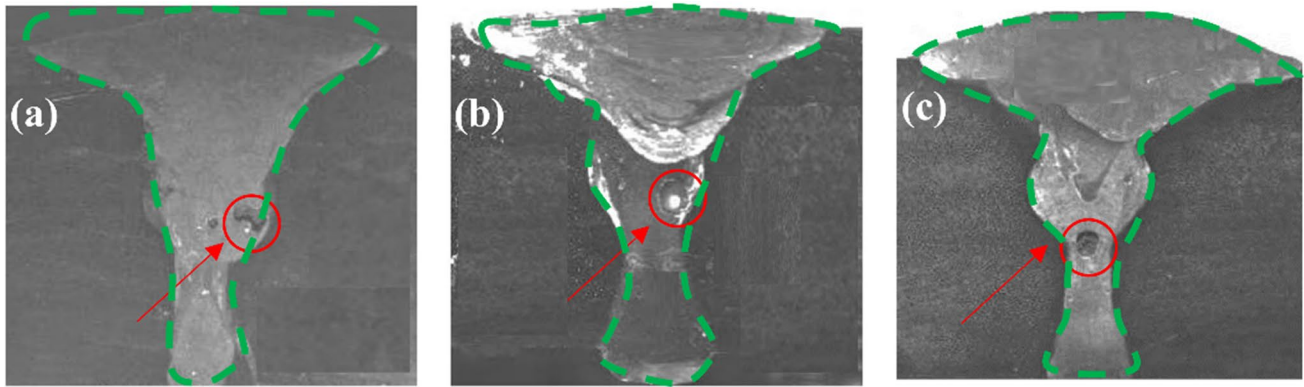


Fig. 25 The type of porosities: **a** interlayer porosity, **b** hydrogen porosity, and **c** process porosity

porosity defects during the welding solidification [90, 97]. When the solidification velocity exceeded the filling velocity of the molten metal for the collapsed keyhole, porosity defects could also be formed [98]. The instability of the keyhole is another main reason for porosity defect formations [99, 100]. The formation of porosity defects had a close relation with the instability of vapor force in the laser keyhole. The droplet transfer mode was a vital factor in influencing the stability of the laser keyhole [101]. Mizutani M et al. [102] found that the keyhole was generated in the liquid molten pool, rather than in a solid metal, and bubbles were usually generated at the top of the keyhole. By using a simplified numerical model to calculate the surface of the molten pool, it was found that the surface tension of the liquid molten pool affected the generation of porosities. The research by Katayama et al. [103] showed that the keyhole was in a drastic fluctuation and unstable state during laser non-penetration welding, and the keyhole experienced periodic collapse and irregular changes. This unstable collapse could envelop the gas inside the keyhole, which led to the formation of keyhole-type porosities during the solidification process. Therefore, the stability of the keyhole is the key to affecting the generation of keyhole-type porosity defects. Xu et al. [104] analyzed the fluidity of the keyhole and molten pool state with a high-speed image system and argued that the erratic fluctuation in the keyhole was the dominant reason to form porosity defects. Wen et al. [105] investigated the effect of laser keyhole dynamic behavior on weld penetration. The results indicated that the effect of pulse frequency on the fluctuation of weld depth was more important than that of laser power and defocusing amount.

Different process parameters also have a vital effect on the formation of porosity defects. The continuous optimization of process parameters can improve the porosity defects. The researchers have carried out experimental studies on different process parameters, as shown in Fig. 26. The following parameters can affect porosity defects in this review and are summarized in Table 4.

The welding speed exerts a significant influence on the formation of porosity. According to Madison et al. [106], the porosity defects decreased with increasing welding speed. While Yu et al. [107] believed that the porosity defects increased as laser power increased. The characteristics of the molten pool depended on the laser energy and welding speed and were related to the formation of porosity defects. Zhan et al. [108] studied the formation mechanism of porosities, and found that the welding speed and keyhole stability were closely related to the formation of porosity defects. High welding speed led to the instability of the keyhole, which promoted the formation of porosities. Katayama et al. [99] believed that porosities would be formed in the middle part of the laser keyhole under the condition of high laser power. At the low welding speed, the porosities would be generated at the bottom part of the keyhole. Bunaziv et al. [109] suggested that the generation of porosity defects had a connection with the behavior of the back wall of the keyhole in LAHW. When the welding speed increased continuously, the inclination angle of the keyhole increased, and the rear wall of the keyhole was prone to collapse due to the instability of the keyhole, which increased the porosity of the welds, as shown in Fig. 27. Leo et al. [93] demonstrated that an appropriate laser-arc power distribution can minimize the porosities of Al-Mg alloy welds with the thickness of 3 mm.

Welding current can influence the molten pool temperature, the molten pool fluidity, and the molten pool wettability. The molten pool temperature will increase with the increasing of the welding current, which makes it easy for the gas inside the molten pool to escape, thereby reducing the formation of porosities. Appropriate welding current can improve the fluidity of the molten pool, which is beneficial for the overflow of porosities. Furthermore, the welding current also affects the molten pool wettability, thereby decreasing the generation of porosity defects. Xu et al. [110] established a three-dimension molten pool flow model, as shown in Fig. 28. It explained the generation mechanism of

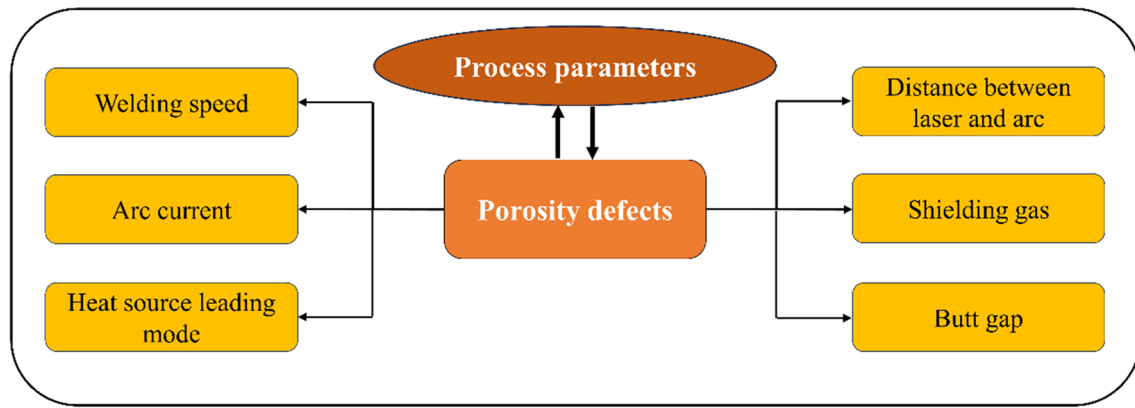


Fig. 26 The process parameters of influencing porosity defects

Table 4 The effect of different process parameters on porosity defects

Process parameters	Welding method	Workpiece	Plate thickness	Laser power	Ref.
Welding speed	Laser welding	304L stainless steel	1 mm	1.2 kW	[106]
	Laser welding	5A06 aluminum alloy	2 mm/4 mm	2.6–4 kW	[107]
	Laser welding	TA15 titanium alloy	5 mm	2–6 kW	[108]
Arc current	Laser welding	304 austenitic stainless steel or aluminum alloy plates	12 mm	10 kW	[99]
	LAHW	High-strength steel	45 mm	15 kW	[109]
	LAHW	Al-Mg alloy	3 mm	2.5–3.5 kW	[93]
	LAHW	Aluminum alloy	-	3.8 kW	[110]
	LAHW	AA6082	8 mm	3 kW	[14]
	Laser welding	AA6061-T6 alloy	6 mm	6 kW	[111]
	Laser welding	316L austenitic stainless steel	10 mm	2.4, 2.7, 3.0 kW	[104]
	LAHW	Low-carbon steel	10 mm	3–4 kW	[112]
	LAHW	HNS	10 mm	4 kW	[113]
	LAHW	5A06 aluminum alloy	6.9 mm	3–3.8 kW	[114]
Heat-source leading mode	LAHW	5083 aluminum alloy	10 mm	3.0, 4.9 kW	[115]
	LAHW	AA5754-H111 Mg-Al alloy	3 mm	3 kW	[116]
Distance between laser and arc	LAHW	Aluminum alloy	6 mm	2.5, 3.0, 3.7, 4.0 kW	[96]
	LAHW	AZ31B magnesium alloy	5 mm	1.5 kW	[117]
	LAHW	5083 aluminum alloy	5 mm	2.5 kW	[118]
Shielding gas	LAHW	Al/steel	1.5 mm	2 kW	[119]
	Laser welding	AA 2024-T3 aluminum, alloy	3 mm	4.9 kW	[120]
	LAHW	A7N01P-T4 aluminum, alloy	12 mm	4 kW	[121]
	LAHW	42CrMo steel	5 mm	3.1, 3.3, 3.5 kW	[122]
Butt gap	Laser welding	5A06 aluminum alloy	2 mm/4 mm	2.6–4 kW	[107]

process-type porosities. At the same time, the experiments were conducted to verify the model, as shown in Fig. 29. The process experiment showed that the porosity decreased from 7.56 to 4.66%, as the arc current increased from 180 to 260 A. The simulation results indicated that the flow direction of the melt around the keyhole was towards the bottom of the welds, and the flow direction changed, which increased surface instability and led to the closure of the upper part

of the keyhole. Due to the buoyancy force of the porosity defects, the distribution of porosity defects in the welds was asymmetric. On the other hand, it was found that the flow velocity on the molten pool surface would reduce when the current increased from 200 to 260 A, which increased the keyhole stability.

Ascari et al. [14] found that the arc current of hybrid welding had a significant impact on the formation of

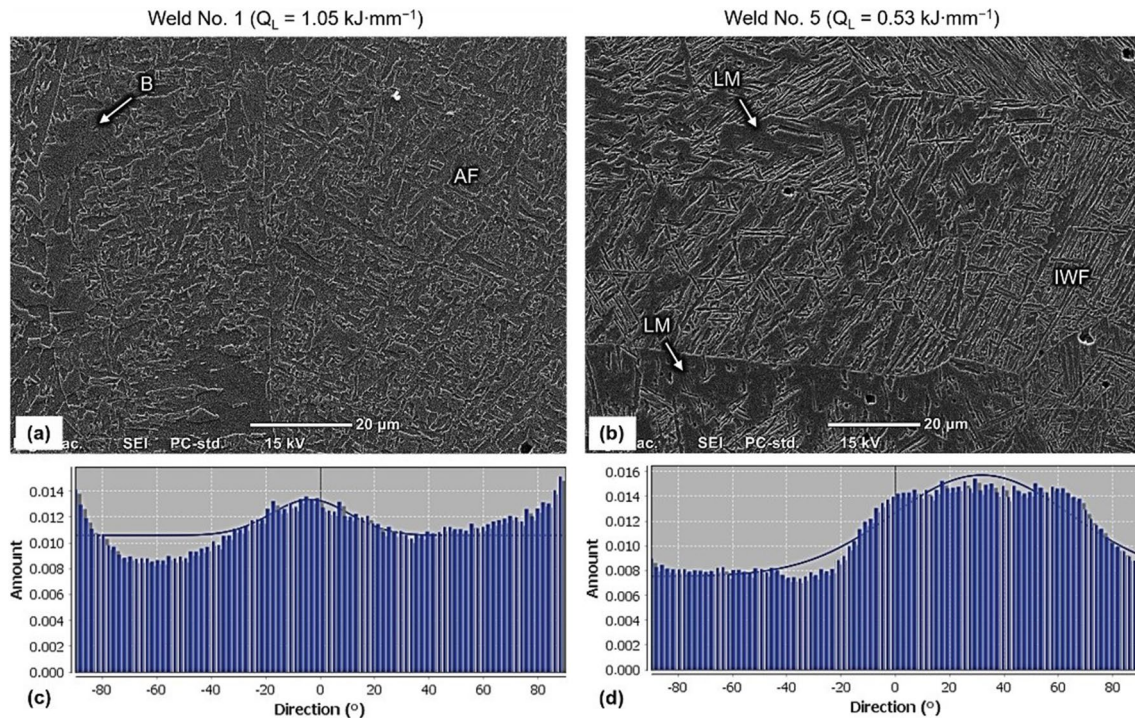


Fig. 27 SEM of microstructure and misorientation angles in the root of **a** and **c** high-heat input and **b** and **d** low-heat input welding [109]

porosity defects, while the D_{LA} had little effect on the porosity defects. Ola et al. [111] found that laser energy and laser beam diameter could affect the morphology of the keyhole, which affected the number of porosities. Xu et al. [104] believed that the merging of bubbles was more intense when energy density was higher, and the possibility of forming porosities increased. The porosity increased and then decreased with the increase of arc current. The arc could drive the liquid metal near the keyhole to block the keyhole and form bubbles, which escaped from the molten pool [112]. Cui et al. [113] investigated the effect of heat input on weld porosity defects. The results showed that weld porosity defects increased as the laser power increased. Zhao et al. [114] thought that high laser power could promote the escape of porosity defects from the molten pool.

Laser welding can effectively control the formation of porosity defects due to its high energy density and focus characteristics. On the contrary, the scattered focus and low energy density of the arc welding, the welding parameters, and shielding gas conditions need to be adjusted more carefully to reduce the generation of porosity defects. Huang et al. [115] adopted laser-leading and arc-leading welding methods to implement experiments, respectively. In the laser-leading welding process, the arc became more divergent, the keyhole was less prone to collapse, and the bubbles were more likely to escape from the molten pool, which effectively suppressed the formation of metallurgical and process porosity defects. In the mechanical performance test,

the tensile strength of welding joints obtained by laser-leading and arc-leading methods can reach 90.3 and 87.9% of the base metal, respectively. This was related to the smaller porosity (Fig. 30), smaller grain size (Fig. 31), more precipitation of second phases and dislocation lines (Fig. 32), and less Mg element burning loss during laser-leading welding. Casalino et al. [116] found that the molten pool was more stable in laser-leading welding mode, with fewer keyhole collapses, and fewer porosity defects than in arc-leading welding mode.

A large D_{LA} may lead to insufficient filling of the welds, which limits the fluidity of the molten pool, making it difficult to expel gas from the welding area. In this case, there is a greater risk of porosity formation. On the contrary, a small D_{LA} may promote sufficient filling of the molten pool, which is beneficial for the uniform distribution of heat, and makes it easier for gas to be discharged from the welding area. Ola et al. [96] conducted bead-on-plate welding on a 6-mm thickness 2024 aluminum alloy and statistically analyzed the porosity defects. The study found that the D_{LA} had a significant impact on the welding penetration and porosity. As the D_{LA} increased from 1 to 5 mm, the weld penetration increased and then decreased. When the D_{LA} was 2 mm, the coupling effect of the laser-arc heat source was best with the smallest penetration, but the porosity also changed with the change of penetration. The depth of penetration was proportional to the porosity quantity. Chen et al. [117] studied the effect of process parameters on the stability of

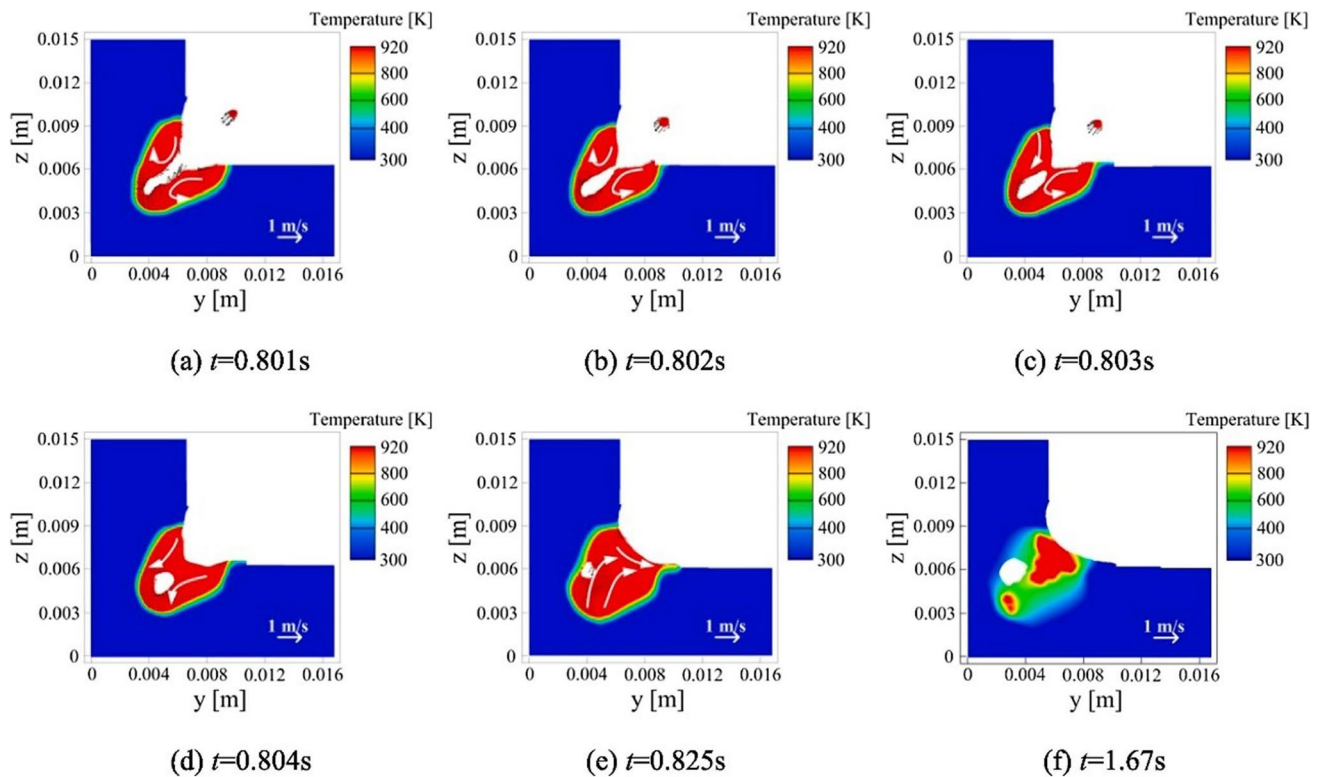


Fig. 28 The formation process of keyhole-induced bubble and porosity at weld pool cross-sections [110]

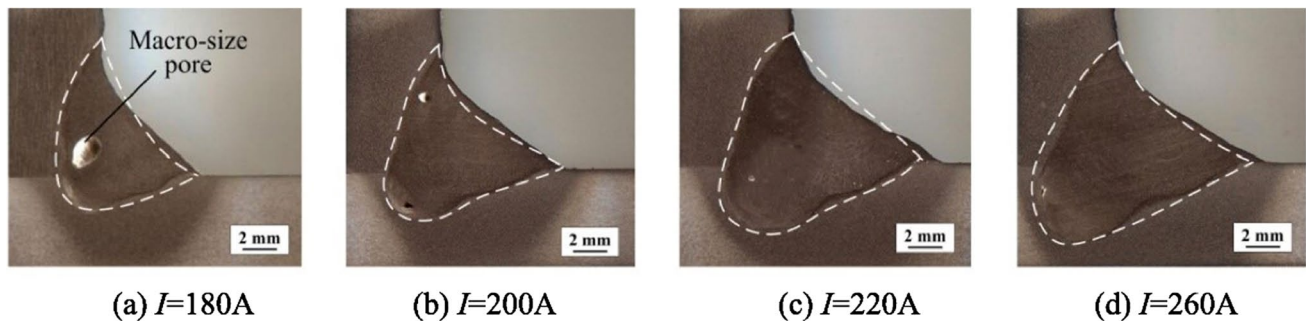


Fig. 29 Weld cross sections for different welding currents [110]

the keyhole and analyzed the principle of porosity formation. The results showed that porosity defects in hybrid welding usually appeared at the bottom of the welds, and a large weld depth-to-width ratio would make joint porosity defects increase. In addition, the relative position of the laser and arc heat source also exerted a significant influence on the generation of porosity defects. Bunaziv et al. [118] found that aluminum alloy was more prone to generate porosity defects compared with steel, as shown in Fig. 33. Since aluminum alloy had physical properties with good fluidity, low melting point, and low surface tension, They mainly investigated the effect of D_{LA} on porosity defects. Although there was an optimal value, there was still a 15% porosity rate.

One of the main functions of shielding gas is to prevent oxygen from entering the welding area, which reduces the formation of oxides. By using appropriate shielding gas, the formation of oxides can be effectively reduced, which improves the weld quality. Choosing the proper type and flow rate of shielding gas can help minimize porosities and enhance the compactness of the welds. Furthermore, the fluidity and stability of the shielding gas can help maintain the stability of the molten pool. A stable molten pool helps to expel gas and reduce the generation of porosity defects. Sun et al. [119] showed that the shielding gas composition greatly affected the formation of porosity defects. When N_2 was utilized as a shielding gas, it could suppress the porosity

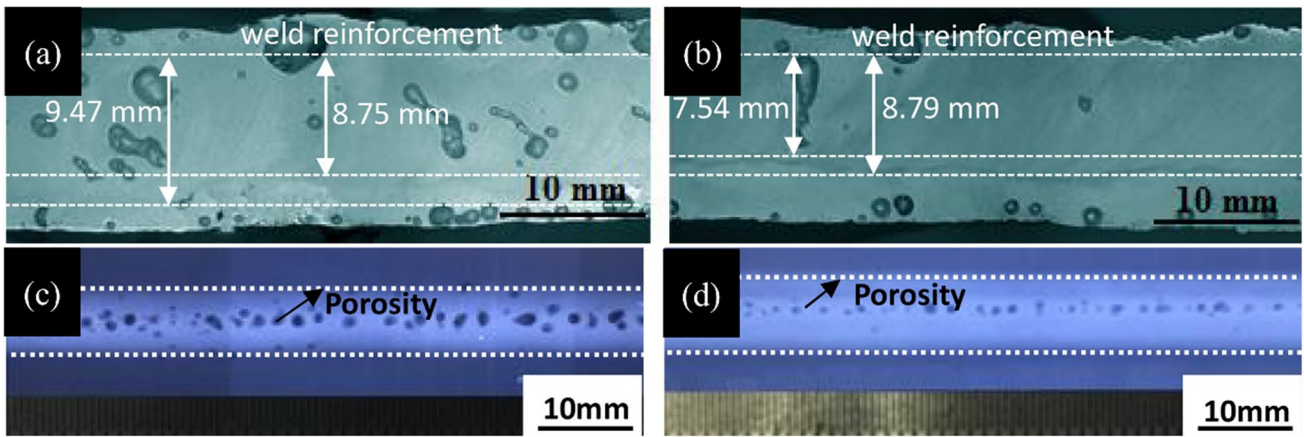


Fig. 30 The longitudinal sections of the weld beads and X-ray radiographs of welds **a–c** ALHW and **b–d** LAHW [115]

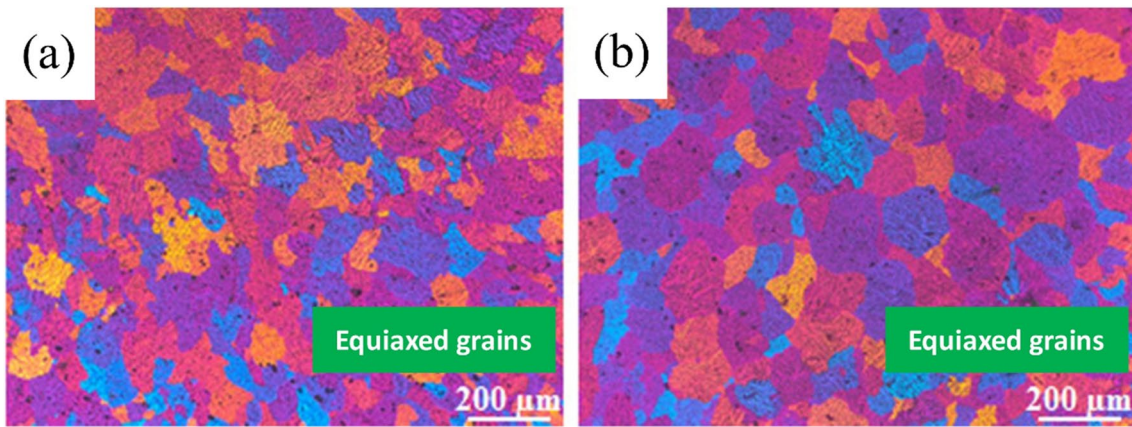


Fig. 31 Grain size of equiaxed grain zone in the center of the welds **a** ALHW and **b** LAHW[115]

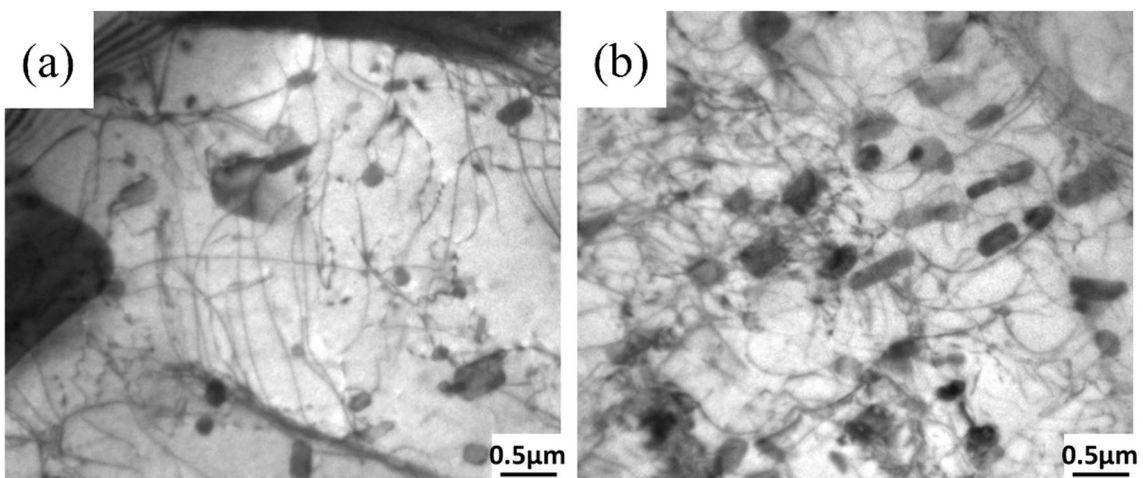


Fig. 32 The density of dislocation in the WZ: **a** ALHW and **b** LAHW[115]

defects of the welds. Ahn et al. [120] concluded that the thermal conductivity of helium increased the welds width, molten pool temperature, and solidification time when helium was utilized as the shielding gas, which was helpful to the escape of porosities from the molten pool, as shown in Fig. 34. Chuang et al. [121] argued that the mixed shielding gas of argon and helium improved the keyhole stability and effectively suppressed the formation of porosities during LAHW. When the helium volume ratio was 50%, it could improve the penetration depth significantly and inhibit porosities. Zhang et al. [122] argued that increasing the flow rate of shielding gas was beneficial to reduce porosity defects.

The butt gap has a certain impact on the formation of porosities and welding quality. Yu et al. [107] pointed out that the generation of porosities has a close relation with the stability of keyholes and the flow of the molten pool. The addition of welding wire will affect the keyhole stability and cause the molten pool fluctuation, making it easier to produce porosity defects. For flat plate butt joints, remaining appropriate butt gaps can provide a channel for bubbles to escape and a flow space for molten metal, increasing the stability of the keyhole and molten pool. If the butt gap is large, the amount of material filled in the welds will increase, and more molten metal is needed to fill the gap. A large butt gap may lead to insufficient heat input in the welding area, poor fluidity of the molten metal, and increase the risk of porosity formation. A small butt gap is beneficial for the uniform distribution of heat input in the welding area and the sufficient filling of molten metal, which can decrease the generation of porosity defects. Therefore, in actual welding, the appropriate butt gap should be determined based on welding requirements and material characteristics.

The oscillation laser welding technology, in which the laser beam moves by swinging or scanning during the welding process. The oscillation laser welding can affect the formation of porosity defects. Compared with conventional

laser welding, oscillation laser welding has many superiorities, including increasing assembly tolerance, improving weld formation and joint performance, and inhibiting welding porosity [123–125]. Wang et al. [126] showed that the porosity defects were effectively hindered when oscillating laser welding method was utilized. Hao et al. [127] found that beam oscillation parameters had a suppression effect on the porosity defects, as shown in Fig. 35. Miyagi et al. [128] studied the effects of scanning laser frequency and amplitude on the surface discontinuities and porosity in welds. In conventional laser welding, the weld penetration depth was large and the weld width was small. When the keyhole was open and close, the gas would enter into the root of the keyhole. The gas was not easy to be discharged when the molten pool cooled rapidly and formed porosity defects. After scanning, the molten pool would be stirred to reduce the depth of the keyhole and increase the weld width, which was helpful to the spread of the molten pool and the floating of bubbles. However, under high-frequency scanning, the excessively high frequency could cause sever stirring of the molten pool, which was not conducive to the stability of the welding process.

In oscillation laser welding, the choice of laser power and frequency will affect the weld width and the formation of the molten pool. If laser power is quite low or the frequency is much low, it may cause excessive heat input of the molten pool, which makes it difficult for gas to escape from the welds, thereby increasing the possibility of porosity defects. In addition, the amplitude and speed of the oscillation laser will also influence the molten pool fluidity. Proper oscillation amplitude and speed can help the molten metal fully fill the welds, which is conducive to the discharge of gas from the welds, and reduce the generation of porosity defects.

The LAHW has a strong synergistic effect of two heat sources, which may reduce the porosity of welds. This integration of laser and arc welding technology helps to enhance the gap-bridging ability and can decrease the

Fig. 33 The effect of heat source distance and MIG torch direction on weld appearance and quality [118]

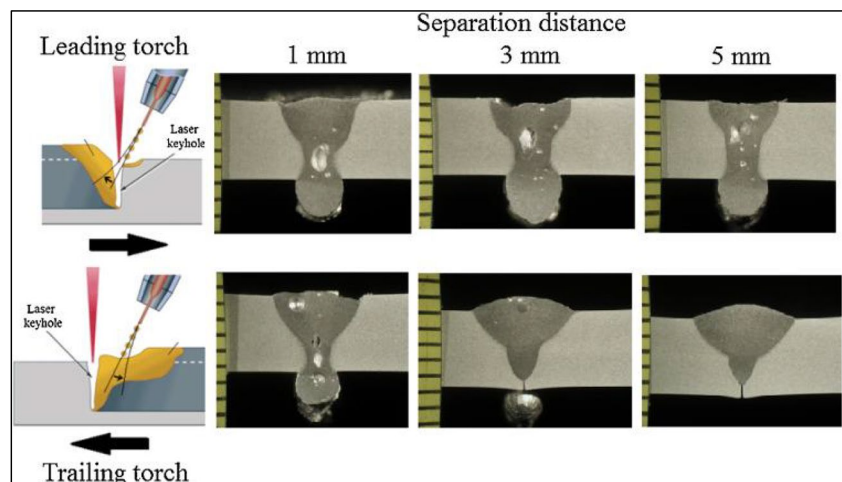
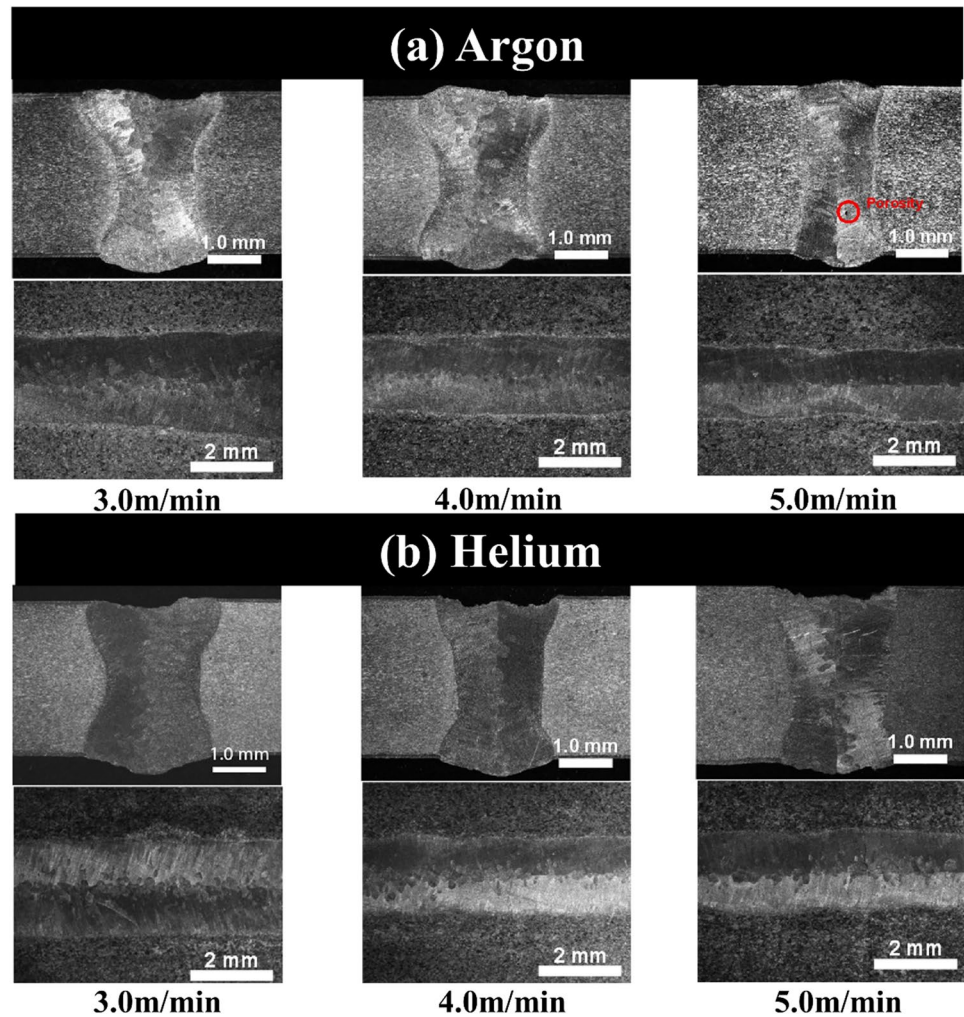


Fig. 34 Transverse sections of welds under different shielding gas: **a** argon and **b** helium [120]



accuracy requirements. Due to the utilize of welding wires, the chemical composition of welds has been improved [129]. In LAHW, a laser beam with high energy density irradiates metal materials, forming a keyhole through reaction pressure and pushing surrounding molten materials. The keyhole is kept open by the reaction pressure generated by the non-equilibrium evaporating particles. During the welding process, excessive pressure generated by the metal vapor can cause instability and collapse of the keyhole, and the metal vapor and shielding gas at the root of the keyhole are involved in the molten pool to generate porosity defects [130].

4.4 Spatter defects

The spatter defect is the fusion of the welding wire and welded workpiece. Under the action of arc force, the droplets formed by the melting welding wire cause spatters around the molten pool, and the molten metal flying outside the molten pool is called spatter defects. Spatter defects not only

seriously affect the surface forming quality of base metal but also affect the surface treatment of the workpiece and subsequent accessory installation.

Many scholars have conducted relevant research on the spatter generation mechanism and analyzed the formation of spatter defects from different perspectives, as shown in Fig. 36. On the one hand, from the force state of the droplet, it is believed that metal vapor reaction force could affect spatter defects. The vapor shear force and the surface tension co-determined the spatter defects [131, 132]. On the other hand, from the flow situation of the molten pool, it is believed that the dynamic behavior of the molten pool was a critical factor that affected the generation of spatter defects [82, 133, 134].

In the first place, from the perspective of droplet force state analysis, the spatter defects have a connection with the droplet force condition. In addition, the mechanism of spatter defects has also been studied. Specifically, the material located at the front of the keyhole is vaporized due to overheating. Because of the volume expansion during the gasification process, the momentum of the molten metal

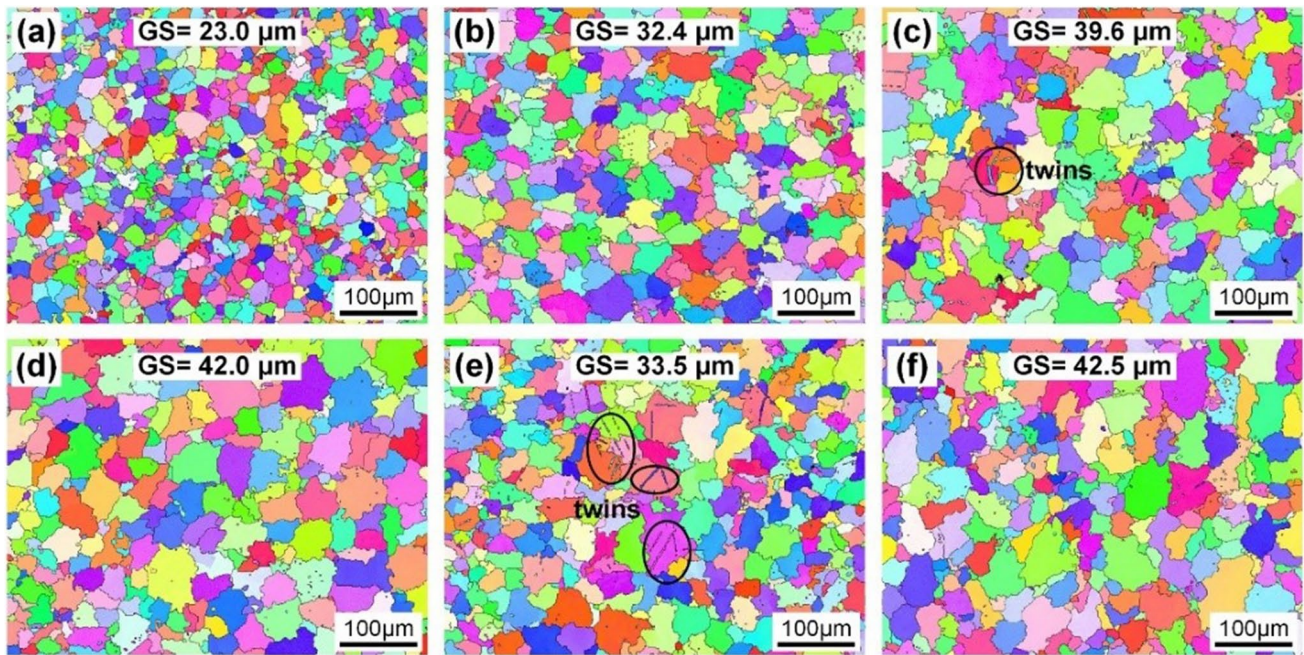


Fig. 35 Inverse pole figures IPFs of the welds, **a** without oscillation, **b** $r = 0.75$ mm and $f = 25$ Hz, **c** $r = 0.75$ mm and $f = 75$ Hz, **d** $r = 0.75$ mm and $f = 150$ Hz, **e** $r = 0.25$ mm and $f = 75$ Hz, and **f** $r = 1.25$ mm and $f = 75$ Hz [127]

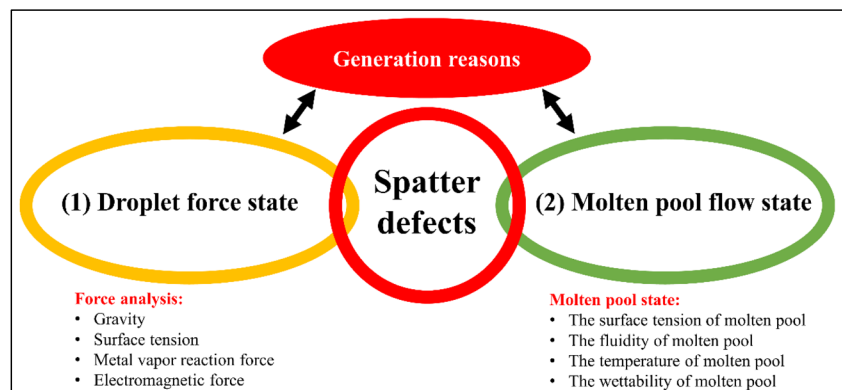
increases. The molten metal flows toward the back of the molten pool. The molten metal located on the surface of the molten pool flows at high speed. After reaching the critical force and speed, molten metal overcomes the constraint of the surface tension of the molten pool to form a liquid column with certain spatial characteristics. After detachment, it forms spatter defects. It can be concluded that the factors that cause the spatter are the inherent characteristics of the vapor flow in the keyhole and molten pool.

Nakamura et al. [135] utilized a fiber laser to join titanium plates with a thickness of 6 mm and adopted different welding speeds to study the generation of spatter. The research showed that the spatter was formed between the keyhole and the solid–liquid interface, and the time was about 20 ms. When the welding speed was less than 50 mm/s, 80%

of the spatters were generated on the front wall of the keyhole. When the welding speed further increased, the number of spatters occurring at the back of the keyhole increased significantly, and the average size was less than 1 mm. Wu et al. [136] studied the formation of spatter defects on the keyhole wall through numerical simulation and high-speed image method. They found that metal vapor shear stress in the keyhole was an important factor in causing the generation of spatter defects, as shown in Fig. 37.

In the second place, from the perspective of the molten pool flow state, it can be seen that the spatter defects are related to the molten pool temperature, the molten pool surface tension, the molten pool wettability, and the molten pool fluidity. Excessive temperature can lead to excessive liquefaction of the molten metal, which reduces surface

Fig. 36 The main generation reasons for spatter defects in this review



tension and increases the possibility of spatter defects. When the surface tension of the molten pool is large, the molten metal is more likely to form small spatters. If the wettability between the molten pool and the workpieces is poor, it may make the molten metal unstable and prone to the generated spatter defects. The molten pool fluidity also affects the generation of spatter defects. When the fluidity of the molten pool is poor, the molten metal may stay on the welds' surface, which forms large droplets and spatters.

Fabbro et al. [137, 138] used high-speed images to study the generation mechanism of spatter defects and believed that the main reason for the spatter was the expansion of metal vapor caused by laser irradiation. The molten metal was affected by the impact force, and the direction of the impact force was vertical upward, so spatter defects were generated. The coupling effect of the steam plume and molten pool flow accelerated the flow of molten metal near the molten pool and keyhole. The surface of the molten pool presented many chaotic surface undulations, and the droplets generated dramatic fluctuations around the keyhole, which led to the formation of a liquid column. After the impact of metal vapor on the front wall of the keyhole, the spatter defects were generated, as shown in Fig. 38. M. Wahbaa et al. [139] utilized 100% CO₂ instead of Ar shielding gas to reduce the cost, optimize weld formation, and reduce spatter. The results indicated that the change in the heat source leading mode had a positive effect on improving weld formation. A laser keyhole located at an appropriate distance behind the arc can adjust the arc length, thereby causing disturbance to the melt flow and eliminating the interference of arc short-circuit on the melt flow. As a result, a high-quality welding joint was obtained, greatly reducing the size and quantity of spatter defects, as shown in Fig. 39. Li et al. [140] utilized a novel and intuitive X-ray transmission image technology

to study the influence of spatter defects and molten pool behavior on welding quality. The results showed that the generation of spatter defects had a close connection with the flow behavior of the molten pool. An increasing in laser power would cause stronger metal evaporation, resulting in more molten metal being extruded. The different types of spatters were formed due to changes in the focal position of the laser beam. The prerequisite for obtaining a stable keyhole was that the laser focus position was located inside the metal, as shown in Fig. 40.

Y Kawahito et al. and S Katayama et al. [141, 142] conducted a study on the molten pool dynamic behavior. The study showed that metal vapor inside the keyhole was ejected towards the oblique rear of the keyhole, and the strong shear force generated by the injection squeezed the back of the keyhole. Similarly, the protrusion phenomenon of molten metal appeared at the back of the molten pool and then separated from the molten pool under force, which formed a large volume spatter. When welding speed and spot diameter are 6m/min and 560 μm, respectively, the influence of different laser incidence angles on the spatter defects was studied. When the laser inclination angle was 0°, the keyhole was located in front of the molten pool, and the melt was blown out from the keyhole, which formed spatter defects. The prerequisite for reducing the number of spatter defects was that the incidence angle of the laser beam would need to be tilted towards the side of the molten pool. When the laser inclination angle is 20°, it was found that the melt sprayed out from the keyhole opening under the combined action of shear force and laser-induced plume.

Zhang et al. [143] analyzed the reasons for spatter formation, compared laser-cold metal transfer (CMT) hybrid welding with laser-MAG hybrid welding, and believed the transfer mode of CMT is short-circuit transfer; the impact

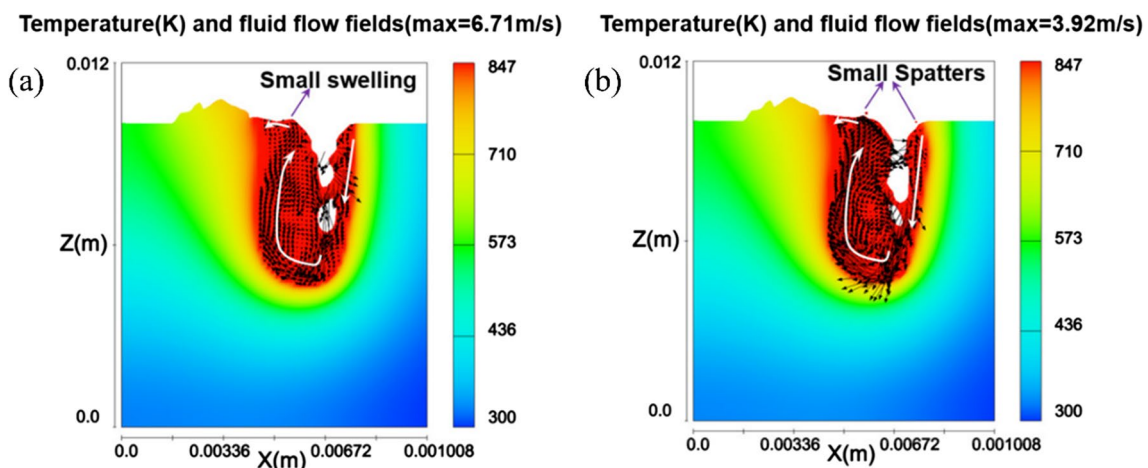


Fig. 37 Temperature °K and fluid flow fields of $y = 0$ cross-sectional view simulation without considering vapor shear stress at **a** $t = 0.113$ s and **b** $t = 0.116$ s [136]

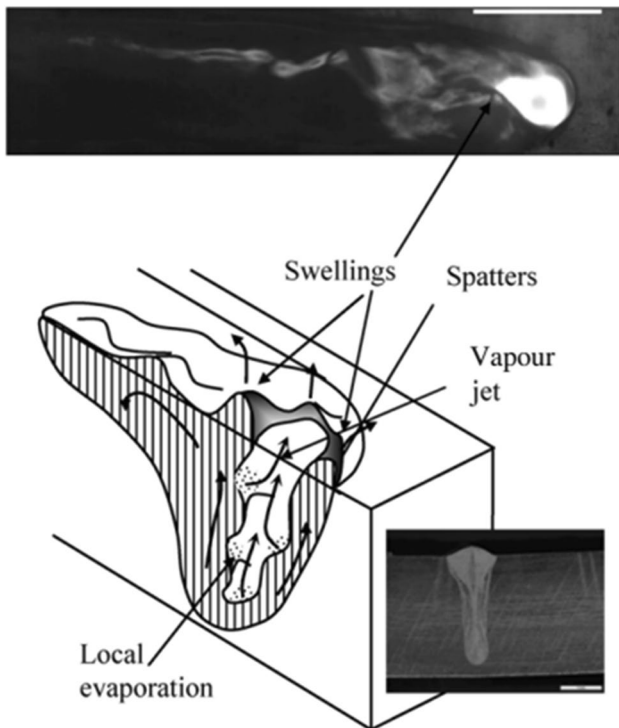


Fig. 38 The formation mechanism of spatter [138]

of molten pool and the mutual interference between arc and laser were reduced, resulting in a significant reduction in spatter and porosity defects. Zhang et al. [144] studied the effect of welding speed on the spatter defect formation on the keyhole wall. They found that the spatter defects were mainly generated on the front wall of the keyhole during the high-speed welding, with a small size and fast movement speed. On the contrary, the spatter defects were mainly produced on the rear wall of the keyhole during the low-speed welding, with large size and slow movement speed.

There are two main reasons for spatter defects in LAHW. First, the spatter is caused by droplet transfer. During the droplet transfer process, the liquid droplet flows through the liquid bridge, causing a short-circuit transfer mode. The

short-circuited bridge overheats and explodes, which causes the liquid metal to contract sharply under the electromagnetic contraction force. With the increase of current and the decrease of necking, the liquid bridge is continuously heated, which causes energy accumulation, and the liquid bridge generates a gasification explosion, resulting in a good number of spatters. Secondly, molten metal flows with the change in the molten pool temperature. There is a metal vapor force near the laser keyhole, and the liquid metal sprays out with the metal vapor force, forming spatters. The generation of spatter defects can reduce the quality of the welds and may cause defects such as the surface collapse of the welds.

5 Defects suppression methods

5.1 Thermodynamic balance method

The hybrid form of LAHW determines the coupling mode of laser-induced plasma and arc plasma, which influences the current path, arc force, and droplet transfer mode directly. Therefore, by changing the hybrid form and welding method of LAHW, or external magnetic field to achieve the control of droplet transfer, arc force, and keyhole morphology, the formation of welding defects can be effectively suppressed. It is an important way to obtain hybrid welding joints with excellent performance. The specific improvement forms can adopt laser-multi-arc hybrid welding, laser-pulse-arc hybrid welding, laser-CMT hybrid welding, and double-sided transverse laser-arc hybrid welding.

Laser-multi-arc hybrid welding adopts a symmetrical arc distribution method. The purpose of this method is to balance the force of laser-induced plasma on the arc, improving the droplet transfer mode, and making the welding process more stable and efficient. Laser-pulse arc/CMT hybrid welding mainly improves arc behavior and droplet transfer mode, reduces welding heat input, and improves the microstructure and properties of welding joints. Laser-pulse multi-arc hybrid welding combines the advantages of the above two methods, and its characteristics are more outstanding.

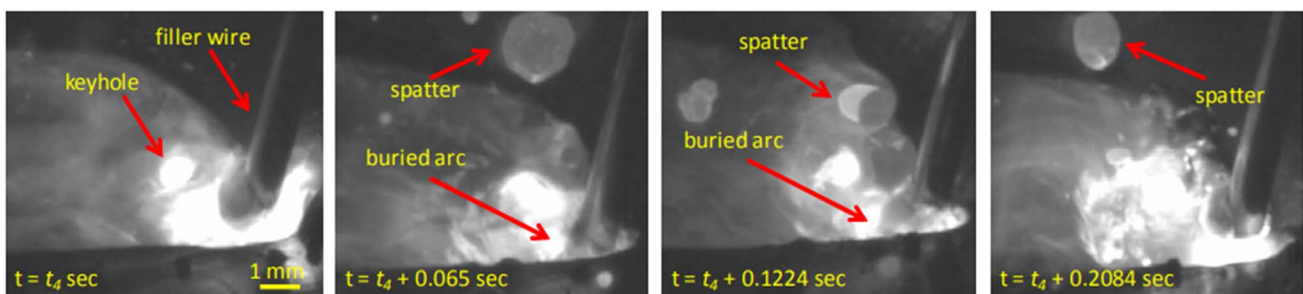
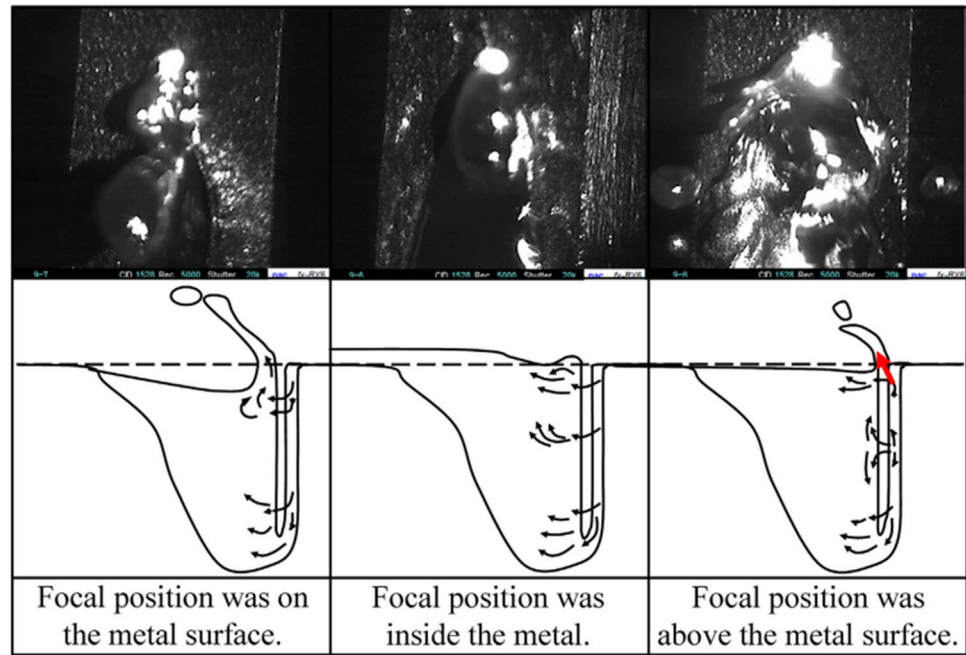


Fig. 39 The influence of arc-leading mode on metal transfer and spatter formation [139]

Fig. 40 Schematic illustration of molten pool behavior under different focal positions [140]



5.2 Improving metallurgical atmosphere method

The shielding gas is one of the critical welding factors for achieving effective LAHW and achieving maximum efficiency. It not only plays a protective role in the metallurgical process and prevents oxidation of the molten pool and burning of alloy elements but also affects the droplet transfer mode and the distribution of welding arc morphology and energy. It can also change the surface tension state of the solid, liquid, and gas interfaces, thereby suppressing the formation of welding defects.

The shielding gas is a quite significant process parameter, and it has a vital influence on the welding joint quality [145]. The shielding gas can remove the plasma shielding effect and improve the welding stability. At the same, in arc welding, the shielding gas can achieve stable arc combustion. In LAHW, shielding gas plays a key role in the weld quality [139, 146]. Most scholars have carried out a large number of experiments about the effect of shielding gas on welding stability [30, 147–149]. Zhu et al. [150] found different droplet transfer modes under different shielding gases in LAHW. When the shielding gas was Ar + 30% He, the droplet transfer was stable. Pan et al. [82] compared the influence of different gas compositions on the welding joint defects. It could be found that optimal shielding gas composition could reduce the generation of spatter defects significantly. Cai et al. [121] found that the He content had a relation with the formation of porosity defects. When 50% He was added to the shielding gas, the porosity defects could be reduced, obviously.

The shielding gas can prevent oxygen from entering the welding area, thereby reducing the formation of oxides.

Oxides are common weld defects in the welding process, which can reduce the welds' strength. Through utilizing the appropriate shielding gas, the formation of oxides can be effectively reduced, thereby improving the quality of welds. The shielding gas can restrain the generation of porosity defects. Choosing the proper type and flow rate of shielding gas can help minimize porosity and improve weld quality. The fluidity of the shielding gas can control the shape of the welds. When using a suitable shielding gas flow rate, better weld morphology can be obtained, which improves the appearance and mechanical properties of the welds. The shielding gas can reduce the HAZ (heat-affected zone). By using shielding gas to reduce the oxygen content in the welding area, the formation of oxides in HAZ can be reduced, and the properties of the material can be improved.

5.3 Finite element analysis and prediction method

Welding finite element analysis is a beneficial tool for understanding the whole physical phenomena and the basic mechanism of the welding process. It is also a convenient and efficient method for optimizing welding structure and process design, avoiding welding defects, and improving the quality of welding joints. A numerical model can assist in process development and enhance understanding of the complex phenomena in the LAHW process.

In order to compensate for the lack of process test or detection, it is essential to utilize numerical simulation method to study physical mechanisms. There are numerous researches on the numerical simulation of welding [151–155]. Du et al. [156] developed a thermos-metallurgical finite element

mode to predict the phase field and molten pool dimensions of steel plates. It can be found that the numerical model could guide the LAHW process. Wu et al. [157] developed a numerical simulation to observe the keyhole dynamic, which laid the foundation for improving the process parameters in LAHW. Kong et al. [158] developed a numerical study to observe higher residual stress distribution in the welding process. It could be seen that welding distortion was related to welding speed. Gao [159] established a two-dimensional thermoelastic plastic model of the welding HAZ and simulated the liquefaction crack behavior with the finite element method. It could be found that the driving force of welding liquefaction cracks was related to the local stress. The tendency of liquefaction cracks could be quantitatively analyzed by the strain rate and the geometric shape of the molten pool during solidification, which explained that LAHW has lower sensitivity to liquefaction cracks than single laser welding. Xu et al. [160] developed a three-dimensional finite element model for aluminum alloy T-joints. The welding temperature field and residual stress deformation caused by heat energy were calculated using a thermal-mechanical sequential coupling algorithm. The results indicated that there was high residual stress in the weld zone and HAZ and a large deformation occurred in the middle and rear of the welds. Kim et al. [161] utilized a three-dimensional thermoelastic plastic model based on the finite element method to predict the deformation and residual stress distribution of LAHW joints. By comparing the trends and amplitudes of welding deformation caused by different laser and arc heat input ratios, the effectiveness and universality of the heat input model were verified. Finally, the welding deformation was well-controlled through the optimal heat input ratio.

The finite element analysis method is a universal numerical analysis technique that utilizes a finite number of computational elements to analyze the stress, deformation, and possibility of structure failure. It simplifies the simulation calculation of complex engineering structures under actual stress conditions and can predict the performance, deformation, and component failure.

6 Conclusions and future outlooks

6.1 Conclusion

There is a growing number of researches in the review aimed at analyzing the formation mechanism of welding defects, and how they can be suppressed or avoided by changing process parameters and observing through online detection technology. In fact, for high-speed welding and thick-plate welding, the lack of stability of the LAHW process has been widely considered as a significant issue that deserves

abundant research. The continuous development and innovation of defects detection technologies are regarded as key factors to push forward the industrial breakthrough of the LAHW process. This review summarized some conclusions as follows:

- (1) The welding defects online detection technology can timely detect welding defects, so as to take measures to improve welding defects, which ensures the quality and integrity of the welds. Handling welding defects can avoid structural failure caused by welding quality issues, which ensures the safety and reliability of the structure. In addition, the welding defects detection technology can reduce unqualified products, and costs. By monitoring and analyzing defects in the welding process, welding parameters and processes can be timely adjusted to improve the stability and consistency of welding quality.
- (2) Based on online detection technology, all kinds of detection technologies have been widely applied to analyze and understand the generation mechanism of welding defects, such as undercut, humping, porosity, and spatter defects.
- (3) Abundant experiment researches have summarized plenty of advanced defect suppression methods, which integrate visual analysis technologies and finite element analysis methods, in order to restrain the generation of welding defects. More and more scholars began to learn deeply to explore and extract complex characteristics of welding mechanisms.

The LAHW process not only involves a variety of field interactions, such as flow field, temperature field, and stress field but also the heat and mass transfer behavior of the solid–liquid–gas evolution of metal materials which is very complex. Therefore, the metal melting and solidification process is quite easy to generate surface defects, such as undercut defects, humping defects, porosity defects, and spatter defects, which cause serious hidden dangers to the reliability of long-term service of welds.

6.2 Future outlooks

At present, researches and applications of LAHW are increasingly attracting widespread attention from industry and scholars. With the diversification of heat sources hybrid form and welding materials, and the further development of science and technology, the research on LAHW will focus on the following aspects:

- (1) The coupling effect between laser-arc hybrid plasma and molten pool plays a decisive role in the formation and development of welding defects, such as undercut,

humping, porosity, and spatter defects. Therefore, further research is carried out on the interaction mechanism and heat sources' hybrid form in order to more accurately reveal the generation of welding defects, which fundamentally suppresses the formation of welding defects and fully utilizes the characteristics of large depth-to-width ratio, high welding speed, and narrow HAZ in LAHW.

- (2) The theoretical system of the hybrid form, plasma morphology, droplet transfer, and numerical simulation of LAHW heat sources needs to be further improved. At the same time, the research on the LAHW process and related finite element numerical simulation urgently needs to be carried out deeply, in order to break through the limitations of experimental conditions and defects detection methods. It provides accurate and reliable theoretical references and data support for the development of new structures, methods, and processes.
- (3) The high-energy density of LAHW makes it possible to break through the efficiency and quality dilemma in thick-plate welding. The use of narrow gap grooves and high-speed welding may become the focus of LAHW technology and theoretical research, as well as numerical simulation.

Authors' contribution Conceptualization: Q.L.; methodology: Q.L.; investigation: Q.L., D.W., P.Z., Q.W., and H.Y.; formal analysis: Q.L.; writing—original draft: Q.L.; data curation: D.W.; supervision: D.W.; writing—review and editing: D.W., R.L., and P.Z.; visualization: P.Z. and T.S.; validation: P.Z.; and funding acquisition: P.Z. All authors have read and agreed to the published version of the manuscript.

Funding This research was supported by the National Natural Science Foundation of China (52075317), the China Postdoctoral Science Foundation (2022T150400), the Class III Peak Discipline of Shanghai—Materials Science and Engineering (high-energy beam intelligent processing and green manufacturing), and the Natural Science Foundation of Shanxi Province (No.202203021211151).

Declarations

Conflict of interest The authors declare no competing interests.

References

1. Casalino G, Campanelli SL, Ludovico AD (2013) Laser-arc hybrid welding of wrought to selective laser molten stainless steel. *Int J Adv Manuf Technol* 68:209–216. <https://doi.org/10.1007/s00170-012-4721-z>
2. Turichin G, Kuznetsov M, Tsibulskiy I, Firsova A (2017) Hybrid laser-arc welding of the high-strength shipbuilding steels: equipment and technology. *Phys Procedia* 89:156–163. <https://doi.org/10.1016/j.phpro.2017.08.005>
3. Petring D (2013) Developments in hybridisation and combined laser beam welding technologies. *Handbook of laser welding technologies*. Elsevier Inc., pp 478–504. <https://doi.org/10.1533/9780857098771.3.478>
4. Chen M, Xu J, Xin L, Zhao Z, Wu F (2016) Comparative study on interactions between laser and arc plasma during laser-GTA welding and laser-GMA welding. *Opt Lasers Eng* 85:1–8. <https://doi.org/10.1016/j.optlaseng.2016.04.006>
5. Zhou J, Tsai HL, Wang PC (2012) Hybrid laser-arc welding of aerospace and other materials. *Welding Joining Aerosp Mater*:109–141. <https://doi.org/10.1533/9780857095169.1.109>
6. Wu D, Zhang P, Yu Z, Gao Y, Zhang H, Chen H et al (2022) Progress and perspectives of in-situ optical monitoring in laser beam welding: Sensing, characterization and modeling. *J Manuf Process* 75:767–791. <https://doi.org/10.1016/j.jmapro.2022.01.044>
7. ISOE (2005) Welding - fusion-welded joints in steel, nickel, titanium and their alloys (beam welding excluded) - quality levels for imperfections
8. Ai Y, Jiang P, Wang C, Mi G, Geng S, Liu W et al (2018) Investigation of the humping formation in the high power and high speed laser welding. *Opt Lasers Eng* 107:102–111. <https://doi.org/10.1016/j.optlaseng.2018.03.010>
9. Niu P, Li R, Fan Z, Cao P, Zheng D, Wang M et al (2023) Inhibiting cracking and improving strength for additive manufactured AlxCoCrFeNi high entropy alloy via changing crystal structure from BCC-to-FCC. *Addit Manuf* 71. <https://doi.org/10.1016/j.addma.2023.103584>
10. Shinohara Y, Madi Y, Besson J (2016) Anisotropic ductile failure of a high-strength line pipe steel. *Int J Fract* 197:127–145. <https://doi.org/10.1007/s10704-015-0054-x>
11. Caccese V, Blomquist PA, Berube KA, Webber SR, Orozco NJ (2006) Effect of weld geometric profile on fatigue life of cruciform welds made by laser/GMAW processes. *Mar Struct* 19:1–22. <https://doi.org/10.1016/j.marstruc.2006.07.002>
12. Steen WM (1980) Arc augmented laser processing of materials. *J Appl Phys* 51:5636–5641. <https://doi.org/10.1063/1.3275660>
13. Wang JY, Qi T, Zhong CL, Zhang H, Li XR, Liu FD (2021) Study on seam nitrogen behavior of high nitrogen steel hybrid welding. *Optik (Stuttg)* 242. <https://doi.org/10.1016/j.ijleo.2021.167026>
14. Ascari A, Fortunato A, Orazi L, Campana G (2012) The influence of process parameters on porosity formation in hybrid LASER-GMA welding of AA6082 aluminum alloy. *Opt Laser Technol* 44:1485–1490. <https://doi.org/10.1016/j.optlastec.2011.12.014>
15. Kurzynowski T, Gruber K, Stopyra W, Kuźnicka B, Chlebus E (2018) Correlation between process parameters, microstructure and properties of 316 L stainless steel processed by selective laser melting. *Mater Sci Eng A* 718:64–73. <https://doi.org/10.1016/j.msea.2018.01.103>
16. Gao M, Tang HG, Chen XF, Zeng XY (2012) High power fiber laser arc hybrid welding of AZ31B magnesium alloy. *Mater Des* 42:46–54. <https://doi.org/10.1016/j.matdes.2012.05.034>
17. Gao Y, Hao K, Xu L, Han Y, Zhao L, Ren W et al (2022) Microstructure homogeneity and mechanical properties of laser-arc hybrid welded AZ31B magnesium alloy. *J Mag Alloys*. <https://doi.org/10.1016/j.jma.2022.09.034>
18. Yang S, Wang D, Yang L, Zhang F, Zhang C, Zhou B et al (2022) Effects of laser-arc hybrid welding on microstructure and mechanical properties of dissimilar steel joint. *Optik (Stuttg)* 268. <https://doi.org/10.1016/j.ijleo.2022.169795>
19. Li Y, Jiang P, Li Y, Mi G, Geng S (2023) Microstructure evolution and mechanical properties in the depth direction of ultra-high power laser-arc hybrid weld joint of 316L stainless steel.

- Opt Laser Technol 160. <https://doi.org/10.1016/j.optlastec.2022.109093>
20. Saternus Z, Piekarska W, Kubiak M, Domański T, Sowa L (2016) Numerical analysis of deformations in sheets made of X5CRNI18-10 steel welded by a hybrid laser-arc heat source. *Procedia Eng* 136:95–100. <https://doi.org/10.1016/j.proeng.2016.01.180>
 21. Li L, Xia H, Ma N, Pan B, Huang Y, Chang S (2018) Comparison of the welding deformation of mismatch and normal butt joints produced by laser-arc hybrid welding. *J Manuf Process* 34:678–687. <https://doi.org/10.1016/j.jmapro.2018.07.015>
 22. Gu X, Li H, Yang L, Gao Y (2013) Coupling mechanism of laser and arcs of laser-twin-arc hybrid welding and its effect on welding process. *Opt Laser Technol* 48:246–253. <https://doi.org/10.1016/j.optlastec.2012.10.025>
 23. Campana G, Ascari A, Fortunato A, Tani G (2009) Hybrid laser-MIG welding of aluminum alloys: The influence of shielding gases. *Appl Surf Sci* 255:5588–5590. <https://doi.org/10.1016/j.apsusc.2008.07.169>
 24. Swanson PT, Page CJ, Read E, Wu HZ (2007) Plasma augmented laser welding of 6 mm steel plate. *Sci Technol Weld Join* 12:153–160. <https://doi.org/10.1179/174329307X164283>
 25. Gumenyuk A, Rethmeier M (2003) Latest MIG, TIG Arc-YAG laser hybrid welding systems for various welding products. *Proc SPIE - Int Soc Optic Eng* 4831. <https://doi.org/10.1117/12.497771>
 26. Gumenyuk A, Rethmeier M (2013) Developments in hybrid laser-arc welding technology. *Handbook of laser welding technologies*. Elsevier Inc., pp 505–521. <https://doi.org/10.1533/9780857098771.3.505>
 27. Qin GL, Lei Z, Lin SY (2007) Effects of Nd:YAG laser + pulsed MAG arc hybrid welding parameters on its weld shape. *Sci Technol Weld Join* 12:79–86. <https://doi.org/10.1179/174329306X147544>
 28. Fellman A, Kujanpää V (2006) The effect of shielding gas composition on welding performance and weld properties in hybrid CO₂ laser–gas metal arc welding of carbon manganese steel. *J Laser Appl* 18:12–20. <https://doi.org/10.2351/1.2164481>
 29. Heimbs S, Engström H, Nilsson K, Kaplan AFH (2003) Parameter influence in CO₂-laser/MIG hybrid welding. In: Conference: 56th Annual Assembly of the International Institute of Welding
 30. Zhang S, Sun J, Zhu M, Zhang L, Nie P, Li Z (2019) Effects of shielding gases on process stability of 10CrNi3MoV steel in hybrid laser-arc welding. *J Mater Process Technol* 270:37–46. <https://doi.org/10.1016/j.jmatprotec.2019.01.027>
 31. Zhu Y, Cai Y, Dong H, Wang M (2022) Tailoring droplet transfer and molten pool flow during hybrid laser arc welding of nickel base alloy. *Opt Laser Technol*:147. <https://doi.org/10.1016/j.optlastec.2021.107620>
 32. Malinauskas M, Žukauskas A, Hasegawa S, Hayasaki Y, Miz-eikis V, Buividas R et al (2016) Ultrafast laser processing of materials: from science to industry. *Light Sci Appl* 5. <https://doi.org/10.1038/lsa.2016.133>
 33. Penilla EH, Devia-Cruz LF, Wieg AT, Martinez-Torres P, Cuando-Espitia N, Sellappan P et al (2019) Ultrafast laser welding of ceramics. *Science* 365(6455):803–808. <https://doi.org/10.1126/science.aaw6699>
 34. Tetsui T (2001) Effects of brazing filler on properties of brazed joints between tial and metallic materials. *Intermetallics* 9(3):253–260. [https://doi.org/10.1016/S0966-9795\(00\)00129-1](https://doi.org/10.1016/S0966-9795(00)00129-1)
 35. Sheng Z, Xu Y, Guo H, Zhou J, Chang L, Ding W et al (2022) Study on droplet transfer behavior during medium and low power laser assisted pulsed MAG hybrid welding. *Optik (Stuttg)* 270. <https://doi.org/10.1016/j.ijleo.2022.169972>
 36. Zhang W, Hua X, Liao W, Li F, Wang M (2014) Behavior of the plasma characteristic and droplet transfer in CO₂ laser-GMAW-P hybrid welding. *Int J Adv Manuf Technol* 72:935–942. <https://doi.org/10.1007/s00170-014-5731-9>
 37. Račko D (1987) Acoustic emission from welds as indicator of cracking. *Mater Sci Technol (United Kingdom)* 3:1062–1066. <https://doi.org/10.1179/mst.1987.3.12.1062>
 38. Grad L, Grum J, Polajnar I, Slabe JM (2004) Feasibility study of acoustic signals for on-line monitoring in short circuit gas metal arc welding. *Int J Mach Tools Manuf* 44:555–561. <https://doi.org/10.1016/j.ijmactools.2003.10.016>
 39. Nguyen NT, Wahab MA (1996) The effect of undercut and residual stresses on fatigue behaviour of misaligned butt joints. *Eng Fract Mech* 55
 40. Bell R, Vosikovskiy O, Bain SA (1989) The significance of weld toe undercuts in the fatigue of steel plate t-joints. *Int J Fatig* 11(1):3–11. [https://doi.org/10.1016/0142-1123\(89\)90041-8](https://doi.org/10.1016/0142-1123(89)90041-8)
 41. Alam MM, Barsoum Z, Jonsén P, Kaplan AFH, Häggblad HÅ (2010) The influence of surface geometry and topography on the fatigue cracking behaviour of laser hybrid welded eccentric fillet joints. *Appl Surf Sci* 256:1936–1945. <https://doi.org/10.1016/j.apsusc.2009.10.041>
 42. Nguyen TN, Wahab MA (1998) The effect of weld geometry and residual stresses on the fatigue of welded joints under combined loading. *J Mater Proc Technol* 77
 43. Otegui JL, Kerr HW, Burns DJ, Mohaupt UH (1989) Fatigue crack initiation from defects at weld toes in steel. *Int J Press Vessels Pip* 38
 44. Adam N K (1957) Use of the term ‘young’ s equation’ for contact angles. *Nature* 180(4590). <https://doi.org/10.1038/180809a0>
 45. Fernando Mendez P, Eagar T (2000) Humping Formation in High Current GTA Welding. <https://www.researchgate.net/publication/260024051>
 46. Meng X, Qin G, Bai X, Zou Z (2016) Numerical analysis of undercut defect mechanism in high speed gas tungsten arc welding. *J Mater Process Technol* 236:225–234. <https://doi.org/10.1016/j.jmatprotec.2016.05.020>
 47. Hu Z, Hua L, Qin X, Ni M, Ji F, Wu M (2021) Molten pool behaviors and forming appearance of robotic GMAW on complex surface with various welding positions. *J Manuf Process* 64:1359–1376. <https://doi.org/10.1016/j.jmapro.2021.02.061>
 48. Gao Z, Hao K, Xu L, Han Y, Zhao L, Jing H (2023) Undercut inhibition mechanisms during high-speed MAG welding employing plate inclination. *Opt Laser Technol* 158. <https://doi.org/10.1016/j.optlastec.2022.108912>
 49. Inose K, Kanbayashi J, Abe D, Matsumoto N, Nakanishi Y (2013) Design and welding method for high-strength steel structure using laser-arc hybrid welding. *Weld World* 57:657–664. <https://doi.org/10.1007/s40194-013-0064-0>
 50. Mills KC, Keene BJ (1990) Factors affecting variable weld penetration. *Int Mater Rev* 35(1):185–216. <https://doi.org/10.1179/095066090790323966>
 51. Zong R, Chen J, Wu C (2019) A comparison of TIG-MIG hybrid welding with conventional MIG welding in the behaviors of arc, droplet and weld pool. *J Mater Process Technol* 270:345–355. <https://doi.org/10.1016/j.jmatprotec.2019.03.003>
 52. Mendez PF, Eagar TW (2003) Penetration and defect formation in high current arc welding. Argonne, IL (United States). <https://doi.org/10.2172/835707>
 53. Nguyen TC, Weckman DC, Johnson DA, Kerr HW (2006) High speed fusion weld bead defects. *Sci Technol Weld Join* 11:618–633. <https://doi.org/10.1179/174329306X128464>
 54. Soderstrom E, Mendez P (2006) Humping mechanisms present in high speed welding. *Sci Technol Weld Join* 11:572–579. <https://doi.org/10.1179/174329306X120787>
 55. Alam MM, Kaplan AFH (2012) Analysis of the rapid central melt pool flow in hybrid laser-arc welding. *Phys Procedia* 39:853–862. <https://doi.org/10.1016/j.phpro.2012.10.110>

56. Karlsson J, Norman P, Kaplan AFH, Rubin P, Lamas J, Yañez A (2011) Observation of the mechanisms causing two kinds of undercut during laser hybrid arc welding. *Appl Surf Sci* 257:7501–7506. <https://doi.org/10.1016/j.apsusc.2011.03.068>
57. Normana PM, Karlsson J, Kaplan AFH (2011) Mechanisms forming undercuts during laser hybrid arc welding. *Phys Procedia* 12:201–207. <https://doi.org/10.1016/j.phpro.2011.03.026>
58. Frostevarg J, Kaplan AFH (2014) Undercut suppression in laser-arc hybrid welding by melt pool tailoring. *J Laser Appl* 26. <https://doi.org/10.2351/1.4872062>
59. Eriksson I, Powell J, Kaplan AFH (2013) Melt behavior on the keyhole front during high speed laser welding. *Opt Lasers Eng* 51:735–740. <https://doi.org/10.1016/j.optlaseng.2013.01.008>
60. Michael R, Sergej G, Marco L et al (2009) Laser-hybrid welding of thick plates up to 32 mm using a 20 kW fibre laser. *Quart J Japan Weld Soc* 27(2):74s–79s. <https://doi.org/10.2207/qjwjs.27.74s>
61. Li J, Sun Q, Liu Y, Zhen Z, Sun Q, Feng J (2020) Melt flow and microstructural characteristics in beam oscillation superimposed laser welding of 304 stainless steel. *J Manuf Process* 50:629–637. <https://doi.org/10.1016/j.jmapro.2019.12.053>
62. Tao X, Ba X, Xu G, Liu L (2023) Effect of laser power on pulsed laser-induced MAG hybrid overhead welding of 4-mm-X70 pipeline steel. *Opt Laser Technol*:164. <https://doi.org/10.1016/j.optlastec.2023.109460>
63. Ai Y, Liu X, Huang Y, Yu L (2020) Numerical analysis of the influence of molten pool instability on the weld formation during the high speed fiber laser welding. *Int. J Heat Mass Transf* 160. <https://doi.org/10.1016/j.ijheatmasstransfer.2020.120103>
64. Zhou J, Tsai HL (2008) Modeling of transport phenomena in hybrid laser-MIG keyhole welding. *Int J Heat Mass Transf* 51:4353–4366. <https://doi.org/10.1016/j.ijheatmasstransfer.2008.02.011>
65. Liu G, Tang X, Han S, Lu F, Cui H (2020) Influence of interwire angle on undercutting formation and arc behavior in pulsed tandem narrow-gap GMAW. *Mater Des* 193. <https://doi.org/10.1016/j.matdes.2020.108795>
66. Nguyen TC, Weckman DC, Johnson DA, Kerr HW (2005) The humping phenomenon during high speed gas metal arc welding. *Sci Technol Weld Join* 10:447–459. <https://doi.org/10.1179/174329305X44134>
67. Nguyen TC, Weckman DC, Johnson DA (2007) The discontinuous weld bead defect in high-speed gas metal arc welds. *Weld J* (Miami, Fla) 86
68. Eriksson I, Gren P, Powell J, Kaplan AF (2010) New high-speed photography technique for observation of fluid flow in laser welding. *Opt Eng* 49:1. <https://doi.org/10.1117/1.3502567>
69. Frostevarg J, Norman P, Karlsson J, Kaplan AFH (2009) Monitoring undercut, blowouts and root sagging during laser beam welding. In: *Conference Lasers in Manufacturing*, vol 5. LIM, Munich, Germany. <https://www.researchgate.net/publication/257052247>
70. Kaplan A, Eriksson I, Kaplan AFH, Norman P, Eriksson I (2009) Analysis of the keyhole and weld pool dynamics by imaging evaluation and photodiode monitoring. In: *Proceedings of LAMP2009: The 5th International Congress on Laser Advanced Materials Processing; LPM2009, the 10th International Symposium on Laser Precision Microfabrication; HPL2009, the 5th International Symposium on High Power Laser Processing; Kobe, June 29 - July 2, 2009; [congress program & technical digest]*. Sumitomo Corp., Tokyo
71. Haug P, Rominger V, Speker N, Weber R, Graf T, Weigl M et al (2013) Influence of laser wavelength on melt bath dynamics and resulting seam quality at welding of thick plates. *Phys Procedia* 41:49–58. <https://doi.org/10.1016/j.phpro.2013.03.051>
72. Powell J, Ilar T, Frostevarg J, Torkamany MJ, Na S-J, Petring D et al (2015) Weld root instabilities in fiber laser welding. *J Laser Appl* 27. <https://doi.org/10.2351/1.4906390>
73. Bachmann M, Avilov V, Gumenyuk A, Rethmeier M (2014) Experimental and numerical investigation of an electromagnetic weld pool support system for high power laser beam welding of austenitic stainless steel. *J Mater Process Technol* 214:578–591. <https://doi.org/10.1016/j.jmatprotec.2013.11.013>
74. Avilov VV, Gumenyuk A, Lammers M, Rethmeier M (2012) PA position full penetration high power laser beam welding of up to 30 mm thick AlMg3 plates using electromagnetic weld pool support. *Sci Technol Weld Join* 17:128–133. <https://doi.org/10.1179/1362171811Y.0000000085>
75. Frostevarg J (2018) Factors affecting weld root morphology in laser keyhole welding. *Opt Lasers Eng* 101:89–98. <https://doi.org/10.1016/j.optlaseng.2017.10.005>
76. Palmer TA, Debroy T (2015) Mitigation of root defect in laser and hybrid laser-arc welding. *Welding Journal* 94(3):73S–82S. <https://www.researchgate.net/publication/279321301>
77. Ilar T, Eriksson I, Powell J, Kaplan A (2012) Root humping in laser welding—an investigation based on high speed imaging. *Phys Procedia* 39:27–32. <https://doi.org/10.1016/j.phpro.2012.10.010>
78. Pan Q, Mizutani M, Kawahito Y, Katayama S (2016) High power disk laser-metal active gas arc hybrid welding of thick high tensile strength steel plates. *J Laser Appl* 28:012004. <https://doi.org/10.2351/1.4934939>
79. Zhang M, Chen G, Zhou Y, Liao S (2014) Optimization of deep penetration laser welding of thick stainless steel with a 10kW fiber laser. *Mater Des* 53:568–576. <https://doi.org/10.1016/j.matdes.2013.06.066>
80. Tang G, Zhao X, Li R, Liang Y, Jiang Y, Chen H (2020) The effect of arc position on laser-arc hybrid welding of 12-mm-thick high strength bainitic steel. *Opt Laser Technol* 121. <https://doi.org/10.1016/j.optlastec.2019.105780>
81. Mazar Atabaki M, Ma J, Yang G, Kovacevic R (2014) Hybrid laser/arc welding of advanced high strength steel in different butt joint configurations. *Mater Des* 64:573–587. <https://doi.org/10.1016/j.matdes.2014.08.011>
82. Pan Q, Mizutani M, Kawahito Y, Katayama S (2016) Effect of shielding gas on laser-MAG arc hybrid welding results of thick high-tensile-strength steel plates. *Weld World* 60:653–664. <https://doi.org/10.1007/s40194-016-0333-9>
83. Zhang M, Zhang Y, Mao C, Hu Y, Chen G, Bi Z (2019) Experiments on formation mechanism of root humping in high-power laser autogenous welding of thick plates with stainless steels. *Opt Laser Technol* 111:11–19. <https://doi.org/10.1016/j.optlastec.2018.09.029>
84. Cao X, Wanjara P, Huang J, Munro C, Nolting A (2011) Hybrid fiber laser - arc welding of thick section high strength low alloy steel. *Mater Des* 32:3399–3413. <https://doi.org/10.1016/j.matdes.2011.02.002>
85. Shen X, Li L, Guo W, Teng W, He W (2016) Comparison of processing window and porosity distribution in laser welding of 10 mm thick 30CrMnSiA ultrahigh strength between flat (1G) and horizontal (2G) positions. *J Laser Appl* 28:022418. <https://doi.org/10.2351/1.4943992>
86. Sun J, Feng K, Zhang K, Guo B, Jiang E, Nie P et al (2017) Fiber laser welding of thick AISI 304 plate in a horizontal (2G) butt joint configuration. *Mater Des* 118:53–65. <https://doi.org/10.1016/j.matdes.2017.01.015>
87. Yamba P, Zhenying X, Yun W, Rong W, Xing Y (2019) Investigation of humping defect formation in a lap joint at a high-speed hybrid laser-GMA welding. *Results Phys* 13. <https://doi.org/10.1016/j.rinp.2019.102341>
88. Wang J, Wang C, Meng X, Hu X, Yu Y, Yu S (2012) Study on the periodic oscillation of plasma/vapour induced during high power

- fibre laser penetration welding. *Opt Laser Technol* 44:67–70. <https://doi.org/10.1016/j.optlastec.2011.05.020>
89. Kawaguchi I, Tsukamoto S, Arakane G, Honda H (2006) Characteristics of high-power CO₂ laser welding and porosity suppression mechanism with nitrogen shielding. Study of high-power laser welding phenomena. *Weld Int* 20:100–105. <https://doi.org/10.1533/wint.2006.3541>
 90. Katayama S, Kobayashi Y, Mizutani M, Matsunawa A (2001) Effect of vacuum on penetration and defects in laser welding. *J Laser Appl* 13(5):187–192. <https://doi.org/10.2351/1.1404413>
 91. Matsunawa A, Seto N, Kim J, Mizutania M, Katayama S (1998) Dynamics of keyhole and molten pool in laser welding. *J Laser Appl* 10(6):247–254. <https://doi.org/10.2351/1.521858>
 92. Daugherty WL, Cannell GR (2003) Analysis of porosity associated with Hanford 3013 Outer Container Welds. *Pract Fail Anal* 3
 93. Leo P, Renna G, Casalino G, Olabi AG (2015) Effect of power distribution on the weld quality during hybrid laser welding of an Al-Mg alloy. *Opt Laser Technol* 73:118–126. <https://doi.org/10.1016/j.optlastec.2015.04.021>
 94. Zhang Y, Song X, Chang L, Wu S (2017) Fatigue lifetime of laser-MIG hybrid welded joint of 7075-T6 aluminum alloy by in-situ observation. *Xiyou Jinshu Cailiao Yu Gongcheng/Rare Metal Mater Eng* 46:2411–2416. [https://doi.org/10.1016/s1875-5372\(17\)30207-2](https://doi.org/10.1016/s1875-5372(17)30207-2)
 95. Cho WI, Na SJ, Cho MH, Lee JS (2010) Numerical study of alloying element distribution in CO₂ laser-GMA hybrid welding. *Comput Mater Sci* 49:792–800. <https://doi.org/10.1016/j.commsci.2010.06.025>
 96. Ola OT, Doern FE (2015) Keyhole-induced porosity in laser-arc hybrid welded aluminum. *Int J Adv Manuf Technol* 80:3–10. <https://doi.org/10.1007/s00170-015-6987-4>
 97. Katayama A (2006) Physical phenomena and porosity prevention mechanism in laser-arc hybrid welding. *Tran-JWRI* 10:18910/12224
 98. Mazar Atabaki M, Ma J, Liu W, Kovacevic R (2015) Pore formation and its mitigation during hybrid laser/arc welding of advanced high strength steel. *Mater Des* 67:509–521. <https://doi.org/10.1016/j.matdes.2014.10.072>
 99. Katayama S, Kawahito Y, Mizutani M (2010) Elucidation of laser welding phenomena and factors affecting weld penetration and welding defects. *Phys Procedia* 5:9–17. <https://doi.org/10.1016/j.phpro.2010.08.024>
 100. Tsukamoto S (2011) High speed imaging technique Part 2 - High speed imaging of power beam welding phenomena. *Sci Technol Weld Join* 16:44–55. <https://doi.org/10.1179/136217110X12785889549949>
 101. Yang S, Yang L, Wang D, Zhang F, Liu C, Huang G (2022) Effect of welding stability on process porosity in laser arc hybrid welding of dissimilar steel. *Optik (Stuttg)* 271. <https://doi.org/10.1016/j.ijleo.2022.170165>
 102. Mizutani M, Katayama S, Matsunawa A (2003) Observation of molten metal behavior during laser irradiation: basic experiment to understand laser welding phenomena. *Proc SPIE Int Soc Optic Eng* 4831. <https://doi.org/10.1117/12.497909>
 103. Katayama S, Iviizutanf M, Matsunawa A (2002) Development of porosity prevention procedures during laser welding. In: *First International Symposium on High-Power Laser Macro-processing*, May 27–31, 2002, Osaka, Japan. Joining and Welding Research Institute (JWRI), Osaka University, Osaka, Japan. <http://spiedl.org/terms>
 104. Xu J, Rong Y, Huang Y, Wang P, Wang C (2018) Keyhole-induced porosity formation during laser welding. *J Mater Process Technol* 252:720–727. <https://doi.org/10.1016/j.jmatprotec.2017.10.038>
 105. Sun J, Nie P, Feng K, Li Z, Guo B, Jiang E (2017) The elimination of pores in laser welds of AISI 304 plate using different shielding gases. *J Mater Process Technol* 248:56–63. <https://doi.org/10.1016/j.jmatprotec.2017.05.011>
 106. Madison JD, Aagesen LK (2012) Quantitative characterization of porosity in laser welds of stainless steel. *Scr Mater* 67:783–786. <https://doi.org/10.1016/j.scriptamat.2012.06.015>
 107. Yu Y, Wang C, Hu X, Wang J, Yu S (2010) Porosity in fiber laser formation of 5A06 aluminum alloy. *J Mech Sci Technol* 24:1077–1082. <https://doi.org/10.1007/s12206-010-0309-4>
 108. Zhan X, Yan T, Gao Q, Zhu Z, Bu H, Wang Z (2019) The porosity formation mechanism in the laser welded joint of TA15 titanium alloy. *Mater Res Express* 6. <https://doi.org/10.1088/2053-1591/ab1612>
 109. Bunaziv I, Wenner S, Ren X, Frostevarv J, Kaplan AFH, Akselsen OM (2020) Filler metal distribution and processing stability in laser-arc hybrid welding of thick HSLA steel. *J Manuf Process* 54:228–239. <https://doi.org/10.1016/j.jmapro.2020.02.048>
 110. Xu G, Li L, Wang H, Li P, Guo Q, Hu Q et al (2019) Simulation and experimental studies of keyhole induced porosity in laser-MIG hybrid fillet welding of aluminum alloy in the horizontal position. *Opt Laser Technol* 119. <https://doi.org/10.1016/j.optlastec.2019.105667>
 111. Ola OT, Doern FE (2017) Factors controlling keyhole-induced porosity in cold wire laser welded aluminum. *J Laser Appl* 29:012008. <https://doi.org/10.2351/1.4967510>
 112. Zou J, Zhao Z, Kong H, Wang Z, Jiang F (2023) Keyhole mouth instability and pore formation in fiber laser-arc hybrid manufacturing. *Opt Laser Technol* 164. <https://doi.org/10.1016/j.optlastec.2023.109561>
 113. Cui B, Liu S, Zhang F, Luo T, Feng M (2022) Effect of welding heat input on pores in laser-arc hybrid welding of high nitrogen steel. *Int J Adv Manuf Technol* 119:421–434. <https://doi.org/10.1007/s00170-021-08113-z>
 114. Zhao Y, Zhan X, Zhou X, Liu T, Kang Y (2021) Effect of heat input on macro morphology and porosity of laser-MIG hybrid welded joint for 5A06 aluminum alloy. *Int J Adv Manuf Technol* 115:4035–4045. <https://doi.org/10.1007/s00170-021-07378-8>
 115. Huang L, Wu D, Hua X, Liu S, Jiang Z, Li F et al (2018) Effect of the welding direction on the microstructural characterization in fiber laser-GMAW hybrid welding of 5083 aluminum alloy. *J Manuf Process* 31:514–522. <https://doi.org/10.1016/j.jmapro.2017.12.010>
 116. Casalino G, Campanelli SL, Maso UD, Ludovico AD (2013) Arc leading versus laser leading in the hybrid welding of aluminium alloy using a fiber laser. *Procedia CIRP* 12:151–156. <https://doi.org/10.1016/j.procir.2013.09.027>
 117. Chen M, Li X, Liu L (2012) Effect of electric field on interaction between laser and arc plasma in laser-arc hybrid welding. *IEEE Trans Plasma Sci* 40:2045–2050. <https://doi.org/10.1109/TPS.2012.2199768>
 118. Bunaziv I, Akselsen OM, Salminen A, Unt A (2016) Fiber laser-MIG hybrid welding of 5 mm 5083 aluminum alloy. *J Mater Process Technol* 233:107–114. <https://doi.org/10.1016/j.jmatprotec.2016.02.018>
 119. Xiao M, Gao C, Tan C, Zhao Y, Liu H, Yang J (2021) Experimental and numerical assessment of interfacial microstructure evolution in dissimilar Al/steel joint by diode laser welding-brazing. *Optik (Stuttg)* 245. <https://doi.org/10.1016/j.ijleo.2021.167706>
 120. Ahn J, He E, Chen L, Dear J, Davies C (2017) The effect of Ar and He shielding gas on fibre laser weld shape and microstructure in AA 2024-T3. *J Manuf Process* 29:62–73. <https://doi.org/10.1016/j.jmapro.2017.07.011>
 121. Cai C, He S, Chen H, Zhang W (2019) The influences of Ar-He shielding gas mixture on welding characteristics of fiber laser-MIG hybrid welding of aluminum alloy. *Opt Laser Technol* 113:37–45. <https://doi.org/10.1016/j.optlastec.2018.12.011>
 122. Zhang Y, Chen G, Mao S, Zhou C, Chen F (2017) Optimization of hybrid laser arc welding of 42CrMo steel to suppress pore formation. *Appl Phys A Mater Sci Process* 123. <https://doi.org/10.1007/s00339-017-1004-4>
 123. Schultz V, Seefeldt T, Vollertsen F (2018) Gap bridging ability in laser beam welding of thin aluminum sheets. *Laser Institute of America*, pp 1165–1173. <https://doi.org/10.2351/1.5063044>

124. Fetzter F, Sommer M, Weber R, Weberpals JP, Graf T (2018) Reduction of pores by means of laser beam oscillation during remote welding of AlMgSi. *Opt Lasers Eng* 108:68–77. <https://doi.org/10.1016/j.optlaseng.2018.04.012>
125. Wang L, Gao M, Zhang C, Zeng X (2016) Effect of beam oscillating pattern on weld characterization of laser welding of AA6061-T6 aluminum alloy. *Mater Des* 108:707–717. <https://doi.org/10.1016/j.matdes.2016.07.053>
126. Wang Z, Oliveira JP, Zeng Z, Bu X, Peng B, Shao X (2019) Laser beam oscillating welding of 5A06 aluminum alloys: microstructure, porosity and mechanical properties. *Opt Laser Technol* 111:58–65. <https://doi.org/10.1016/j.optlastec.2018.09.036>
127. Hao K, Gao Y, Xu L, Han Y, Zhao L, Ren W et al (2022) Beam oscillating parameters on pore inhibition, recrystallization and grain boundary characteristics of laser-arc hybrid welded AZ31 magnesium alloy. *J Magnes Alloys*. <https://doi.org/10.1016/j.jma.2022.10.010>
128. Miyagi M, Zhang X, Kawahito Y, Katayama S (2017) Surface void suppression for pure copper by high-speed laser scanner welding. *J Mater Process Technol* 240:52–59. <https://doi.org/10.1016/j.jmatprotec.2016.09.008>
129. Gao Z, Shao X, Jiang P, Wang C, Zhou Q, Cao L et al (2016) Multi-objective optimization of weld geometry in hybrid fiber laser-arc butt welding using Kriging model and NSGA-II. *Appl Phys A Mater Sci Process* 122. <https://doi.org/10.1007/s00339-016-0144-2>
130. Tucker JD, Nolan TK, Martin AJ, Young GA (2012) Effect of travel speed and beam focus on porosity in alloy 690 laser welds. *JOM* 64:1409–1417. <https://doi.org/10.1007/s11837-012-0481-3>
131. Gunenthiram V, Peyre P, Schneider M, Dal M, Coste F, Koutiri I et al (2018) Experimental analysis of spatter generation and melt-pool behavior during the powder bed laser beam melting process. *J Mater Process Technol* 251:376–386. <https://doi.org/10.1016/j.jmatprotec.2017.08.012>
132. Li S, Deng Z, Deng H, Xu W (2017) Microstructure and properties of weld joint during 10 kW laser welding with surface-active element sulfur. *Appl Surf Sci* 426:704–713. <https://doi.org/10.1016/j.apsusc.2017.07.262>
133. Lamas J, Karlsson J, Norman P, Powell J, Kaplan AFH, Yañez A (2013) The effect of fit-up geometry on melt flow and weld quality in laser hybrid welding. *J Laser Appl* 25:032010. <https://doi.org/10.2351/1.4799556>
134. Gao X, Sun Y, Katayama S (2014) Neural network of plume and spatter for monitoring high-power disk laser welding. *Int J Precis Eng Manuf - Green Technol* 1:293–298. <https://doi.org/10.1007/s40684-014-0035-y>
135. Nakamura H, Kawahito Y, Nishimoto K, Katayama S (2015) Elucidation of melt flows and spatter formation mechanisms during high power laser welding of pure titanium. *J Laser Appl* 27. <https://doi.org/10.2351/1.4922383>
136. Wu D, Hua X, Ye Y, Huang L, Li F, Huang Y (2018) Experimental and numerical study of spatter formation and composition change in fiber laser welding of aluminum alloy. *J Phys D Appl Phys* 51. <https://doi.org/10.1088/1361-6463/aab758>
137. Fabbro R, Slimani S, Doudet I, Coste F, Briand F (2006) Experimental study of the dynamical coupling between the induced vapour plume and the melt pool for Nd-Yag CW laser welding. *J Phys D Appl Phys* 39:394–400. <https://doi.org/10.1088/0022-3727/39/2/023>
138. Fabbro R (2010) Melt pool and keyhole behaviour analysis for deep penetration laser welding. *J Phys D Appl Phys* 43. <https://doi.org/10.1088/0022-3727/43/44/445501>
139. Wahba M, Mizutani M, Katayama S (2015) Hybrid welding with fiber laser and CO₂ gas shielded arc. *J Mater Process Technol* 221:146–153. <https://doi.org/10.1016/j.jmatprotec.2015.02.004>
140. Li S, Chen G, Katayama S, Zhang Y (2014) Relationship between spatter formation and dynamic molten pool during high-power deep-penetration laser welding. *Appl Surf Sci* 303:481–488. <https://doi.org/10.1016/j.apsusc.2014.03.030>
141. Kawahito Y, Mizutani M, Katayama S (2009) High quality welding of stainless steel with 10 kW high power fibre laser. *Sci Technol Weld Join* 14:288–294. <https://doi.org/10.1179/136217108X372531>
142. Katayama S, Kawahito Y (2009) Elucidation of phenomena in high-power fiber laser welding and development of prevention procedures of welding defects. *Fiber Lasers VI: Technol Syst Appl* 7195:71951R. <https://doi.org/10.1117/12.807211>
143. Zhang C, Li G, Gao M, Yan J, Zeng XY (2013) Microstructure and process characterization of laser-cold metal transfer hybrid welding of AA6061 aluminum alloy. *Int J Adv Manuf Technol* 68:1253–1260. <https://doi.org/10.1007/s00170-013-4916-y>
144. Zhang G, Zhu B, Zou J, Wu Q, Xiao R (2020) Correlation between the spatters and evaporation vapor on the front keyhole wall during fiber laser keyhole welding. *J Mater Res Technol* 9:15143–15152. <https://doi.org/10.1016/j.jmrt.2020.10.103>
145. Liu Q, Wu D, Wang Q, Zhang P, Yan H, Sun T et al (2023) Research status of stability in dynamic process of laser-arc hybrid welding based on droplet transfer behavior: a review. *Coatings* 13. <https://doi.org/10.3390/coatings13010205>
146. Kah P, Salminen A, Martikainen J (2011) The analysis of shielding gases in laser-arc hybrid welding processes. *Proc Inst Mech Eng B J Eng Manuf* 225:1073–1082. <https://doi.org/10.1177/2041297510393809>
147. Campana G, Fortunato A, Ascari A, Tani G, Tomesani L (2007) The influence of arc transfer mode in hybrid laser-mig welding. *J Mater Process Technol* 191:111–113. <https://doi.org/10.1016/j.jmatprotec.2007.03.001>
148. Ming G, Xiaoyan Z, Qianwu H (2007) Effects of gas shielding parameters on weld penetration of CO₂ laser-TIG hybrid welding. *J Mater Process Technol* 184:177–183. <https://doi.org/10.1016/j.jmatprotec.2006.11.019>
149. Cai C, Li L, Tai L (2017) Narrow-gap laser-MIG hybrid welding of thick-section steel with different shielding gas nozzles. *Int J Adv Manuf Technol* 92:909–916. <https://doi.org/10.1007/s00170-017-0179-3>
150. Zhu Y, Cai Y, Wang M (2022) Effects of He content in shielding gases on high-efficient hybrid laser arc welding with C-276 filler metal. *J Mater Process Technol* 299. <https://doi.org/10.1016/j.jmatprotec.2021.117367>
151. Kik T, Görka J (2019) Numerical simulations of laser and hybrid S700MC T-joint welding. *Materials* 12. <https://doi.org/10.3390/ma12030516>
152. Long H, Gery D, Carlier A, Maropoulos PG (2009) Prediction of welding distortion in butt joint of thin plates. *Mater Des* 30:4126–4135. <https://doi.org/10.1016/j.matdes.2009.05.004>
153. Deng D, Murakawa H (2008) Finite element analysis of temperature field, microstructure and residual stress in multi-pass butt-welded 2.25Cr-1Mo steel pipes. *Comput Mater Sci* 43:681–695. <https://doi.org/10.1016/j.commatsci.2008.01.025>
154. Singh B, Singhal P, Saxena KK (2019) ScienceDirect investigation of thermal efficiency and depth of penetration during GTAW process. *Mater Today Proc* 18(2019):2962–2969. <https://doi.org/10.1016/j.matpr.2019.07.166>
155. Wang L, Chen J, Wu CS, Luan SC (2020) Numerical analysis of arc and droplet behaviors in gas metal arc welding with external compound magnetic field. *J Mater Process Technol* 282. <https://doi.org/10.1016/j.jmatprotec.2020.116638>
156. Du Z, Sun X, Ng FL, Chew Y, Tan C, Bi G (2021) Thermo-metallurgical simulation and performance evaluation of hybrid laser arc welding of chromium-molybdenum steel. *Mater Des* 210. <https://doi.org/10.1016/j.matdes.2021.110029>
157. Wu CS, Zhang HT, Chen J (2017) Numerical simulation of keyhole behaviors and fluid dynamics in laser-gas metal arc hybrid

- welding of ferrite stainless steel plates. *J Manuf Process* 25:235–245. <https://doi.org/10.1016/j.jmapro.2016.11.009>
158. Kong F, Ma J, Kovacevic R (2011) Numerical and experimental study of thermally induced residual stress in the hybrid laser-GMA welding process. *J Mater Process Technol* 211:1102–1111. <https://doi.org/10.1016/j.jmatprotec.2011.01.012>
159. Gao Z (2012) Numerical modeling to understand liquation cracking propensity during laser and laser hybrid welding (I). *Int J Adv Manuf Technol* 63:291–303. <https://doi.org/10.1007/s00170-012-3907-8>
160. Xu G, Wu C, Ma X, Wang X (2013) Numerical analysis of welding residual stress and distortion in laser+GMAW hybrid welding of aluminum alloy T-joint. *Acta Metall Sin (English Letters)* 26:352–360. <https://doi.org/10.1007/s40195-012-0166-5>
161. Kim YC, Hirohata M, Murakami M, Inose K (2015) Effects of heat input ratio of laser–arc hybrid welding on welding distortion and residual stress. *Weld Int* 29:245–253. <https://doi.org/10.1080/09507116.2014.921039>

Publisher's Note Springer Nature remains neutral with regard to jurisdictional claims in published maps and institutional affiliations.

Springer Nature or its licensor (e.g. a society or other partner) holds exclusive rights to this article under a publishing agreement with the author(s) or other rightsholder(s); author self-archiving of the accepted manuscript version of this article is solely governed by the terms of such publishing agreement and applicable law.